Instabilities of spin torque driven auto-oscillations of a ferromagnetic disk magnetized in plane

D. Mancilla-Almonacid and R. E. Arias

Departamento de Física, CEDENNA, Facultad de Ciencias Físicas y Matemáticas, Universidad de Chile, Casilla 487-3, Santiago, Chile

(Received 5 August 2015; revised manuscript received 19 May 2016; published 16 June 2016)

The stability of the magnetization auto-oscillations of the ferromagnetic free layer of a cylindrical nanopillar structure is studied theoretically using a classical Hamiltonian formalism for weakly interacting nonlinear waves, in a weakly dissipative system. The free layer corresponds to a very thin circular disk, made of a soft ferromagnetic material like Permalloy, and it is magnetized in plane by an externally applied magnetic field. There is a dc electric current that traverses the structure, becomes spin polarized by a fixed layer, and excites the modes of the free layer through the transfer of spin angular momentum. If this current exceeds a critical value, it is possible to generate a large amplitude periodic auto-oscillation of a dynamic mode of the magnetization. We separate our theoretical study into two parts. First, we consider an approximate expression for the demagnetizing field in the disk, i.e., $\vec{H}_D = -4\pi M_z \hat{z}$ or a very thin film approximation, and secondly we consider the effect of the full demagnetizing field, where one sees important effects due to the edges of the disk. In both cases, as the applied current density is increased, we determine the modes that will first auto-oscillate and when these become unstable to the growth of other modes, i.e., their ranges of "isolated" auto-oscillation.

DOI: 10.1103/PhysRevB.93.224416

I. INTRODUCTION

In 1996, Slonczewski [1] and Berger [2] simultaneously discovered the spin transfer torque (STT), a phenomenon in which angular momentum is transferred from a spin polarized current to a ferromagnetic material. This phenomenon is observable at a nanometric scale due to the amounts of current necessary and its effect on the magnetization. Geometries where STT has been observed are nanopillars, magnetic multilayers with point contacts and nanoscale magnetic tunnel junctions. Two qualitatively different types of magnetization dynamics have been studied in relation with STT: induced switching of the magnetization from one equilibrium state to another [3–5], and nano-oscillators [6–8] that evidence auto-oscillations due to a possible antidamping effect of the spin torque. Both types of magnetization dynamics have potential technological applications, like nonvolatile magnetic random access memory (MRAM) [9,10] and tunable high-frequency oscillators [11,12], respectively.

Nanopillars in a basic configuration consist of two ferromagnetic layers separated by a metallic spacer. One of the ferromagnetic layers is called the fixed layer, engineered so that the magnetization remains at an equilibrium configuration and that will spin polarize a current that runs through the device. Then the emergent spin polarized current goes through the metallic spacer that uncouples both ferromagnets, and finally through the so-called free layer made of a soft ferromagnet, influencing its magnetization dynamics via transference of angular momentum.

In this study, we are interested in the magnetization dynamics of the free layer, in particular when it acts as a nano-oscillator. Many works [13–16] have used the macrospin approximation to study the free layer dynamics, i.e., they study the nonlinear dynamics of the uniform magnetization mode, assuming that the magnetization dynamics does not develop nonuniform features. These macrospin studies have had successful in explaining some features of experimental results [17–19], but there are other features that require consideration of nonuniform deviations [20–22]. In particular, for nano-oscillators excited into auto-oscillations by spin torque, the amplitudes of oscillation may be large, attaining a point where they become unstable to the growth of nonuniform modes.

In this study, we first analyze the stability of a uniform periodic auto-oscillation, when the free layer is a thin circular disk magnetized in plane with the aid of a uniform magnetic field applied in plane in a particular direction, using a model for the dynamics of a very thin soft ferromagnetic circular disk disregarding edge effects (the demagnetizing field is approximated by its very thin film limit), and we study the thresholds of instability of nonuniform modes in terms of the parameters of the problem: mainly the current density, applied magnetic field and radius of the disk. The values of these parameters are quite relevant for the magnetization dynamics. The model considers a description of the dynamics in terms of amplitudes of excitations, following a standard Hamiltonian formalism [23–27]. An advantage of the model is that a theoretical analysis of the magnetization dynamics and the thresholds can be done, leading to a better understanding of when and how the macrospin solution becomes unstable. By doing separate numerical checks of the dynamics, we corroborate the theoretical results of the model. Similar studies have been done when the applied magnetic field is perpendicular to the plane of the disk [28,29].

Secondly, we improve the theoretical model by considering the full demagnetizing field within the very thin disk approximation. This allows to better understand the finite size effects of a ferromagnetic disk of nanometric dimensions. We determine the nonuniform equilibrium magnetization under an in plane applied magnetic field, and the linear dynamic modes on top of this configuration, that do agree with previous micromagnetic simulations [30,31]. Within this improved model the previous uniform mode becomes quasiuniform, it still has the lowest frequency, but at small radii, there is a mode of edge character with a frequency very close to the latter one. Indeed, this edge mode has a lower critical current than the quasiuniform mode, thus we studied the range of current densities under which it auto-oscillates in isolation,

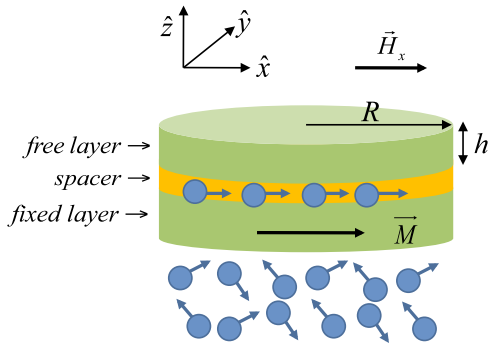

FIG. 1. Representation of a nanopillar and the torque by spin transfer. The electrons are polarized in the fixed layer, go through the spacer, and then produce a torque on the magnetization of the free layer.

and the current under which it becomes unstable to the growth of the quasiuniform mode.

The manuscript is organized as follows. In Sec. II, the model of magnetization dynamics with simplified demagnetizing field is presented; in Sec. III, we develop theoretical results on instability that follow from the simple version of the model; Sec. IV shows applications and numerical results of the simple model; Sec. V shows results for the model with an exact demagnetizing field. Finally, in Sec. VI, we conclude.

II. MODEL, SIMPLER VERSION

The device under study is a nanopillar of circular cross section. In particular, we study the magnetization dynamics of its free layer, which is a thin ferromagnetic disk magnetized in plane. We consider that a spin polarized current runs through the disk, perpendicular to its plane (CPP geometry). The nanopillar is formed by two ferromagnetic layers separated by a metallic spacer. There is a "fixed" ferromagnetic layer with magnetization in the $\hat{x}$ direction (see the geometry in Fig. 1) that serves as spin polarizer for the current that traverses the device. Due to the presence of the spacer, which has to have a certain width, we neglect the Ruderman-Kittel-Kasuya-Yosida (RKKY) interaction between both ferromagnetic layers [32].

We consider that there is a uniform external magnetic field applied in the plane of the free layer (H_x), in direction $\hat{x}$. First, we will approximate the dipolar field by its main term in an infinite very thin ferromagnetic film, i.e., $\vec{H}_D = -4\pi M_z \hat{z}$, assuming that we are dealing with very thin disks (neglected terms are of order h/R). Indeed, we assume that the magnetization is uniform over the thickness of the film, i.e., $\vec{M} = \vec{M}(\vec{\rho})$ with $\vec{\rho} \equiv x\hat{x} + y\hat{y}$, and in particular we do calculations for free layers of Permalloy (exchange length of 5.7 nm) of thickness $h = 5$ nm and radius $R = 50$ nm. Considering the effect of the Zeeman, dipolar and exchange interactions, and the previous approximations, the equilibrium configuration corresponds to a uniform magnetization in the direction of the applied field. The free energy that we consider takes the form $\mathcal{H} = \int \mathcal{W} dV$, with $\mathcal{W}$ the free energy density:

$$\mathcal{W} = -H_x M_x + 2\pi M_z^2 + A \sum_{\alpha=\{x,y,z\}} (\nabla m_\alpha)^2. \qquad (1)$$

A is the exchange constant of the free layer material, M_s the saturation magnetization, and $\vec{m} \equiv \vec{M}/M_s$ a scaled magnetization with norm one ($\vec{m}^2 = 1$). We have neglected an anisotropy energy density since we have a soft ferromagnet in mind, like Permalloy. Thus the effective field associated with this free energy takes the form: $\vec{H}_{\text{eff}} = -\delta\mathcal{H}/\delta\vec{M} = H_x\hat{x} - 4\pi M_z\hat{z} + A\nabla^2\vec{m}$. In order to study, the magnetization dynamics of the free layer, we use the Landau-Lifshitz equation (LL). In addition to the torques associated with the previously mentioned terms (Zeeman, dipolar, exchange), we consider the spin transfer torque associated to the spin polarized current in the form proposed by Slonczewski [33] (in a simple form), and a damping torque in its Landau-Lifshitz phenomenological form [34]. A scaled LLS equation then takes the form:

$$\frac{d\vec{m}}{dt'} = \underbrace{-\vec{m}\times\vec{h}_{\text{eff}}}_{\text{precession}} \underbrace{-\alpha\vec{m}\times(\vec{m}\times\vec{h}_{\text{eff}})}_{\text{dissipation}} + \underbrace{\beta J\vec{m}\times(\vec{m}\times\hat{m}_{\text{fix}})}_{\text{spin transfer torque}}. \qquad (2)$$

Nondimensional quantities have been introduced: $t' = |\gamma|4\pi M_s t$ ($|\gamma|$ is the absolute value of the gyromagnetic ratio), $\vec{h}_{\text{eff}} = \vec{H}_{\text{eff}}/4\pi M_s$, and α is the phenomenological damping constant. Also, $\beta = 2\pi\hbar\epsilon/(4\pi M_s)^2 eh$ [26] (ϵ is the polarization factor between 0 and 1, e is the electron charge, and h the thickness of the free layer, that in the following, we consider fixed), J is the current density, and $\hat{m}_{\text{fix}} = \hat{x}$ is the direction of spin polarization of the current. We also introduce nondimensional frequencies ω, through $\omega = \Omega/|\gamma|4\pi M_s$, with Ω in rad/s.

The previous LLS equation maintains dynamically the restriction $\vec{m}^2 = 1$. Also, since the equilibrium magnetization in this model is $\vec{m} = \hat{x}$, it is convenient to introduce two complex variables $a(\vec{\rho},t)$ and $a^*(\vec{\rho},t)$ that do describe the magnetization dynamics via a classical Holstein-Primakoff transformation [35,36]. a and a^* represent a dynamic perturbation of the equilibrium, and they are the classical analogs of the spin wave annihilation and creation operators of quantum mechanics. The transformation of variables corresponds to

$$\left.\begin{aligned} m_x &= 1 - aa^* \\ m_y &= (a - a^*)\sqrt{2 - aa^*}/2i \\ m_z &= (a + a^*)\sqrt{2 - aa^*}/2 \end{aligned}\right\} \quad \Leftrightarrow \quad a = \frac{m_z + im_y}{\sqrt{1 + m_x}}. \qquad (3)$$

The temporal evolution of the variable a satisfies by the chain rule $i\dot{a} = ida/dt' = i(\partial a/\partial\vec{m})\cdot\dot{\vec{m}}$, and similarly for a^*. Thus, due to this simple dependence on $\dot{\vec{m}}$, the dynamics of the complex variables a and a^* can be obtained through the LLS equation (2) as

$$i\dot{a} = \frac{\delta\mathcal{U}}{\delta a^*} + \mathcal{F}, \qquad (4a)$$

$$i\dot{a}^* = -\frac{\delta\mathcal{U}}{\delta a} - \mathcal{F}^*. \qquad (4b)$$

The first term associated with the normalized free energy $\mathcal{U} \equiv \mathcal{H}/4\pi M_s^2$ corresponds to the conservative precession dynamics in the effective field, and the second term associated with $\mathcal{F}$ corresponds to the dynamics associated with the

Slonczewski spin transfer torque and the Landau-Lifschitz damping. Thus Eqs. (4a) and (4b) have a Hamilton's form (conservative precessional terms) plus nonconservative terms. The different contributing terms can be separated as $\mathcal{U} = \mathcal{U}_Z + \mathcal{U}_D + \mathcal{U}_{\rm ex}$ and $\mathcal{F} = \mathcal{F}_{\rm dis} + \mathcal{F}_{\rm stt}$, with

$$\mathcal{U}_Z = -h_x \int (1 - aa^*) dV, \tag{5a}$$

$$\mathcal{U}_D = \frac{1}{4}\int (a + a^*)^2 \left(1 - \frac{aa^*}{2}\right) dV, \tag{5b}$$

$$\mathcal{U}_{\rm ex} = l_{\rm ex}^2 \int \left\{ \vec{\nabla} a \cdot \vec{\nabla} a^* + \frac{1}{4}\left[a^2 (\vec{\nabla} a^*)^2 + a^{*2} (\vec{\nabla} a)^2 \right] + \frac{aa^*}{8(2 - aa^*)} [\vec{\nabla}(aa^*)]^2 \right\} dV, \tag{5c}$$

with $h_x \equiv H_x/4\pi M_s$, and $l_{\rm ex} \equiv \sqrt{A/2\pi M_s^2}$ the exchange length. And

$$\mathcal{F}_{\rm dis} = i\alpha \left[\frac{\delta \mathcal{U}}{\delta a^*} \left(\frac{8 - 4|a|^2 + |a|^4}{4|a|^2 - 8} \right) + \frac{\delta \mathcal{U}}{\delta a} a^2 \left(\frac{|a|^2 - 4}{4|a|^2 - 8} \right) \right], \tag{6a}$$

$$\mathcal{F}_{\rm stt} = i\beta J a \left(1 - \frac{aa^*}{2} \right). \tag{6b}$$

Furthermore, in order to describe the dynamics in variables suitable to the geometry of the thin disk, we introduce a change of variables from the fields $a(\vec{\rho},t')$,$a^*(\vec{\rho},t')$ to the variables $a_{mj}(t')$,$a^*_{mj}(t')$, which are the coefficients of a Bessel functions series expansion, as follows:

$$a(\vec{\rho},t') = N_{00} a_{00}(t') + \sum_{m=-\infty}^{\infty} \sum_{j=1}^{\infty} N_{mj} a_{mj}(t') J_m(\kappa_{mj}\rho) e^{im\phi}, \tag{7}$$

with ρ and ϕ polar coordinates related to the center of the disk. We also assume that the boundary conditions on the edges of the disk correspond to free spins [37], meaning null normal derivatives of the magnetization on the surfaces of the sample, i.e., in this case, the radial derivatives of the magnetization are null at $\rho = R$, with R the radius of the disk. The latter is satisfied if the κ_{mj} are such that $J'_m(\kappa_{mj} R) = 0$, meaning that $\kappa_{mj} = \chi_{mj}/R$, with χ_{mj} the j^{th} zero of $J'_m(x)$. This series is complete in the mathematical sense, and orthonormal:

$$\int dV J_m(\kappa_{mj}\rho) J_{m'}(\kappa_{m'j'}\rho) e^{i(m+m')\phi} = (-1)^m \delta^m_{-m'} \delta^j_{j'} / N^2_{mj}, \tag{8}$$

$$a_{mj}(t') = N_{mj} \int dV a(\vec{\rho},t) J_m(\chi_{mj}\rho/R) e^{-im\phi}. \tag{9}$$

The normalization coefficients take the following form:

$$N_{00} = 1/\sqrt{V}, \tag{10a}$$

$$N_{mj} = 1/\sqrt{-J_m(\chi_{mj}) J''_m(\chi_{mj}) V}. \tag{10b}$$

These coefficients were chosen in this way so that the transformation from a,a^* to the a_{mj},a^*_{mj} were canonical (considering only the conservative part of the equations). Thus the equations of motion in the new variables take the canonical form with extra terms associated with dissipation and the spin torque term:

$$i\dot{a}_{mj} = \frac{\partial \mathcal{U}}{\partial a^*_{mj}} + \mathcal{F}_{mj}, \tag{11a}$$

$$i\dot{a}^*_{mj} = -\frac{\partial \mathcal{U}}{\partial a_{mj}} - (\mathcal{F}_{mj})^*, \tag{11b}$$

with $\mathcal{F}_{mj} = N_{mj} \int dV \mathcal{F} J_m(\chi_{mj}\rho/R) e^{-im\phi}$.

III. THEORETICAL RESULTS, SIMPLER MODEL

A. Spin wave modes of the equilibrium configuration

The equations of motion satisfied by the linear spin wave modes of the uniform equilibrium configuration correspond to Eqs. (11a) and (11b) excluding the damping and spin torque terms, and follow from the energy $\mathcal{U}$ approximated to quadratic order in the coefficients a_{mj}. Indeed, to this order $\mathcal{U} \simeq \mathcal{U}^{(2)}$, with

$$\mathcal{U}^{(2)} = \sum_{mj} \left[\left(h_x + h^{mj}_{\rm ex} \right) |a_{mj}|^2 + \frac{1}{4} |(a_{mj} + (-1)^m a^*_{-mj})|^2 \right], \tag{12}$$

with $h^{mj}_{\rm ex} \equiv (\chi_{mj} l_{\rm ex}/R)^2$. From Eqs. (11a), (11b), and (12), one obtains

$$i \begin{pmatrix} \dot{a}_{mj} \\ \dot{a}^*_{-mj} \end{pmatrix} = \begin{pmatrix} A_{mj} & (-1)^m B_{mj} \\ -(-1)^m B_{mj} & -A_{mj} \end{pmatrix} \begin{pmatrix} a_{mj} \\ a^*_{-mj} \end{pmatrix} \equiv \mathbf{M} \begin{pmatrix} a_{mj} \\ a^*_{-mj} \end{pmatrix}, \tag{13}$$

with $A_{mj} \equiv h_x + h^{mj}_{\rm ex} + 1/2$ and $B_{mj} = 1/2$. It means that to this order the variables a_{mj} and a^*_{-mj} correspond to two coupled harmonic oscillators. Through the following Bogoliubov transformation [24,38], this problem may be diagonalized:

$$\begin{pmatrix} a_{mj} \\ a^*_{-mj} \end{pmatrix} = \begin{pmatrix} \rho_{mj} & (-1)^m \nu_{mj} \\ (-1)^m \nu_{mj} & \rho_{mj} \end{pmatrix} \begin{pmatrix} b^{(1)}_{mj} \\ b^{(2)}_{mj} \end{pmatrix} \equiv \mathbf{N} \begin{pmatrix} b^{(1)}_{mj} \\ b^{(2)}_{mj} \end{pmatrix} = b^{(1)}_{mj} \begin{pmatrix} \rho_{mj} \\ (-1)^m \nu_{mj} \end{pmatrix} + b^{(2)}_{mj} \begin{pmatrix} (-1)^m \nu_{mj} \\ \rho_{mj} \end{pmatrix}, \tag{14}$$

i.e.,

$$\mathbf{N}^{-1} \mathbf{M} \mathbf{N} = \begin{pmatrix} \omega_{mj} & 0 \\ 0 & -\omega_{mj} \end{pmatrix}, \tag{15}$$

with

$$\rho_{mj} = \sqrt{\frac{A_{mj} + \omega_{mj}}{2\omega_{mj}}}, \qquad \nu_{mj} = \sqrt{\frac{A_{mj} - \omega_{mj}}{2\omega_{mj}}}, \tag{16}$$

$$\omega_{mj} = \sqrt{A^2_{mj} - B^2_{mj}} = \sqrt{\left(h_x + h^{mj}_{\rm ex}\right)\left(h_x + h^{mj}_{\rm ex} + 1\right)}. \tag{17}$$

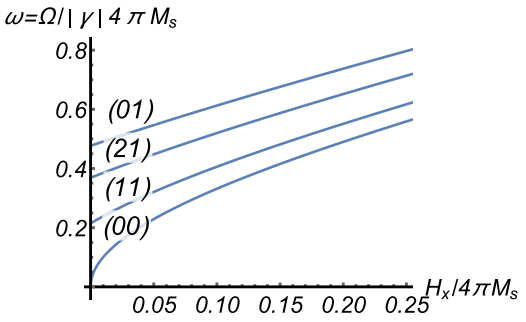

FIG. 2. Frequencies as a function of applied magnetic field for the first four linear modes of the ferromagnetic disk. For a given applied field, the frequency grows for modes with more angular and radial oscillations. Here, ω has no dimensions and Ω has dimensions of rad/s.

There is an analogous transformation to Eq. (14) for the complex conjugates of those variables, i.e., for a^*_{mj}, a_{-mj}, $b^{(1)*}_{mj}$, and $b^{(2)*}_{mj}$. This is a canonical transformation, and the equations of motion in the new variables are

$$i\dot{b}^{(1)}_{mj} = \partial\mathcal{U}/\partial b^{(1)*}_{mj} = \omega_{mj} b^{(1)}_{mj}, \tag{18a}$$

$$i\dot{b}^{(2)}_{mj} = \partial\mathcal{U}/\partial b^{(2)*}_{mj} = -\omega_{mj} b^{(2)}_{mj}, \tag{18b}$$

which have as solutions

$$b^{(1)}_{mj}(t) = b^{0(1)}_{mj}\exp(-i\omega_{mj}t'), \quad b^{(2)}_{mj}(t) = b^{0(2)}_{mj}\exp(i\omega_{mj}t'), \tag{19}$$

with ω_{mj} the normalized frequencies of the normal modes of the disk [Eq. (17), $\omega_{mj} = \Omega_{mj}/|\gamma|4\pi M_s$]. The frequencies increase with the number of radial and angular oscillations of the modes that grow with the indices j and m, as a consequence of the exchange interaction. In Fig. 2, we show a graph of the frequencies as a function of the applied field for the first four modes.

The corresponding shape of the modes follows via Eqs. (7) and (14), noticing that a^*_{mj} and a_{-mj} follow as complex conjugates of the expressions in Eq. (14). If one considers that only the mode (1) exists, and taking $b^{0(1)}_{mj}$ as real, one gets

$$\begin{aligned} m_z &= b^{0(1)}_{mj}\sqrt{2}N_{mj}J_m(\kappa_{mj}\rho)(\rho_{mj}+\nu_{mj})\cos(m\phi-\omega_{mj}t'),\\ m_y &= b^{0(1)}_{mj}\sqrt{2}N_{mj}J_m(\kappa_{mj}\rho)(\rho_{mj}-\nu_{mj})\sin(m\phi-\omega_{mj}t'). \end{aligned} \tag{20}$$

And if only the mode (2) exists, and with $b^{0(2)}_{mj}$ real:

$$\begin{aligned} m_z &= b^{0(2)}_{mj}\sqrt{2}N_{mj}J_m(\kappa_{mj}\rho)(\rho_{mj}+\nu_{mj})\cos(m\phi+\omega_{mj}t'),\\ m_y &= b^{0(2)}_{mj}\sqrt{2}N_{mj}J_m(\kappa_{mj}\rho)(\nu_{mj}-\rho_{mj})\sin(m\phi+\omega_{mj}t'). \end{aligned} \tag{21}$$

Thus these are modes stationary in the radial direction, but that do rotate anticlockwise or clockwise with respect to the angular direction.

If one considers dissipation and the effect of the spin transfer torque, the linear equations (13) lead to

$$i\dot{a}_{mj} = (1-i\alpha)(A_{mj}a_{mj} + B_{mj}(-1)^m a^*_{-mj}) + i\beta J a_{mj}, \tag{22}$$

and to a similar equation for $i\dot{a}^*_{-mj}$. The equation corresponding Eq. (18a) in the variables $b^{(1,2)}_{mj}$ is given by this latter equation with the addition of a term $\mathcal{F}^b_{mj} = \rho_{mj}\mathcal{F}_{mj} - \nu_{mj}(-1)^m {\mathcal{F}_{-mj}}^*$ in the right-hand side (and a similar equation for $\dot{b}^{(2)}_{mj}$). The solution to these equations is

$$\begin{aligned} b^{(1)}_{mj}(t') &\simeq e^{-(\alpha A_{mj}-\beta J)t'}\left(c^0_{mj}e^{-i\omega_{mj}t'} + id^0_{mj}\frac{\alpha B_{mj}}{2\omega_{mj}}e^{i\omega_{mj}t'}\right),\\ b^{(2)}_{mj}(t') &\simeq e^{-(\alpha A_{mj}-\beta J)t'}\left(d^0_{mj}e^{i\omega_{mj}t'} - ic^0_{mj}\frac{\alpha B_{mj}}{2\omega_{mj}}e^{-i\omega_{mj}t'}\right). \end{aligned} \tag{23}$$

Considering low dissipation, i.e., $\alpha \ll 1$, we may approximate

$$\begin{aligned} b^{(1)}_{mj}(t') &\simeq c^0_{mj}e^{-i\omega_{mj}t'}e^{-(\alpha A_{mj}-\beta J)t'},\\ b^{(2)}_{mj}(t') &\simeq d^0_{mj}e^{i\omega_{mj}t'}e^{-(\alpha A_{mj}-\beta J)t'}. \end{aligned} \tag{24}$$

Thus one observes that the spin torque term may act as antidamping, and it leads to auto-oscillations of the mode (m,j) when it compensates the damping at a critical current density $J^{\rm crit}_{mj} = \alpha A_{mj}/\beta$. The lowest critical current density corresponds to the macrospin or uniform mode, with $J^{\rm crit}_{00} = \alpha A_{00}/\beta = \alpha(h_x+1/2)/\beta$. These auto-oscillations of the system can be observed in a range of the applied magnetic field [39,40].

B. Study of the macrospin mode to nonlinear order

As seen in the previous linear analysis of the modes, the macrospin mode enters into an auto-oscillatory regime if the current density exceeds the critical value $J^{\rm crit}_{00} = \alpha(h_x + 1/2)/\beta$, i.e., it exists as an undamped periodic solution. As the current density increases the amplitude of oscillation of the macrospin increases and it will be limited by nonlinear terms. Indeed, the macrospin becomes a periodic nonlinear solution to the equations of motion, which has been studied by several authors [41–45]. In this section, we will present the macrospin solution within the framework of our model. It satisfies the following exact equation [it follows from Eqs. (4a)–(6b)]:

$$\begin{aligned} i\frac{da_{00}}{dt'} &= (1-i\alpha)[(h_x+1/2)a_{00} + a^*_{00}/2] + i\beta J a_{00}\\ &\quad - a_{00}\left(a^2_{00} + 4|a_{00}|^2 + 3{a^*_{00}}^2\right)/8\\ &\quad + i\alpha a_{00}[h_x|a_{00}|^2/2 + (3-|a_{00}|^2)(a_{00}+a^*_{00})^2/8]\\ &\quad - i\beta J a_{00}|a_{00}|^2/2. \end{aligned} \tag{25}$$

In the absence of damping and spin torque, a static solution to this equation is $a^{\rm eq}_{00} = 0$, i.e., $m_x = 1$. We will study the macrospin solution that starts close to $a^{\rm eq}_{00} = 0$ and that grows to nonlinear order and becomes auto-oscillatory in the presence of damping and STT. In order to do so, we introduce the following linear change of variables, $a_{00} = \rho_{00}b_{00} - \nu_{00}b^*_{00}$, with $\rho_{00} = \sqrt{(A_{00}+\omega_{00})/2\omega_{00}}$, $\nu_{00} = \sqrt{(A_{00}-\omega_{00})/2\omega_{00}}$, $A_{00} = h_x + 1/2$, $B_{00} = 1/2$, and $\omega_{00} = \sqrt{h_x(h_x+1)}$. Neglecting

nonresonant terms [this approximation is called rotating wave approximation (RWA)] [46,47], the equation of motion of motion for b_{00} becomes

$$\begin{aligned} i\dot{b}_{00} &= (\omega_{00} - 2A_{00}A_2|b_{00}|^2)b_{00} \\ &\quad - i\alpha A_{00}(1 - A_1|b_{00}|^2 + A_2|b_{00}|^4)b_{00} \\ &\quad + i\beta J(1 - A_3|b_{00}|^2)b_{00}, \end{aligned} \tag{26}$$

with A_1, A_2, and A_3 functions of the applied field (all positive):

$$A_1 = \frac{(A_{00} + 3B_{00})(A_{00} - B_{00})}{2A_{00}\omega_{00}}, \tag{27a}$$

$$A_2 = \frac{B_{00}}{A_{00}} \frac{(2A_{00} - B_{00})(A_{00} - B_{00})}{4\omega_{00}^2}, \tag{27b}$$

$$A_3 = \frac{A_{00}}{2\omega_{00}}. \tag{27c}$$

These previous expressions have been obtained in previous works, like for example Ref. [42], but the nonlinear correction to order 5 in the dissipation is new.

We search for a nonlinear periodic auto-oscillatory solution of Eq. (26), of the form

$$b_{00} = b_{00}^0 e^{-i\omega t'}, \tag{28}$$

with b_{00}^0 a constant, and we obtain

$$\begin{aligned} |b_{00}^0|^2 &= \frac{1}{2A_2/A_3}\big[(A_1/A_3 - J/J_c) \\ &\quad \pm\sqrt{(A_1/A_3 - J/J_c)^2 - 4A_2(1 - J/J_c)/A_3^2}\big], \end{aligned} \tag{29}$$

$$\omega = \left(\omega_{00} - 2A_{00}A_2|b_{00}^0|^2\right), \tag{30}$$

with $J_c = \alpha A_{00}/\beta$ the critical current density. Thus we found an approximate uniform auto-oscillation solution whose frequency diminishes with its amplitude from its linear value ω_{00}.

The nonlinear solution of Eqs. (28)–(30) exists in a certain range of the parameter space (J,h_x). The range of existence of this solution is associated with imposing (i) that $|b_{00}^0|^2$ is real and greater than zero and (ii) that the magnitude of the components of $\vec{m}$ remain in the physical range (in magnitude lower than one). Indeed imposing $m_x(t) = 1 - |a|^2 \geqslant -1$ one gets $|b_{00}^0|^2 \leqslant 2\omega_{00}/(h_x + \sin^2(\omega_{00}t'))$ for all t', which leads to $|b_{00}^0|^2 \leqslant 2\omega_{00}/(h_x + 1)$, i.e., an upper bound for $|b_{00}^0|^2$: we will see that this leads to a maximum current density $J_c^{(1)}(h_x)$ for each applied field h_x.

The analysis of the previous two conditions leads to different allowed solutions depending on the value of the applied field h_x. We will present the different possibilities of solutions fixing the value of h_x at particular ranges and considering the current density to be variable. The ranges of h_x are associated with two special values, $h_x^{(1)} = 1/4$ and $h_x^{(2)}$ which is a solution to the equation $(h_x^{(2)})^3 + h_x^{(2)} - 1/2 = 0$. About the origin of these special h_x field values. (i) If one studies the magnitude of the oscillatory solutions at $J = J_c$, two solutions are obtained $|b_{00}^0|^2 = 0$ and $|b_{00}^0|^2 = (A_1/A_3 - 1)(A_3/A_2)$. The second solution is valid for $A_1/A_3 > 0$, i.e., if $h_x > 1/4$, thus one defines $h_x^{(1)} = 1/4$, which corresponds to $A_1/A_3 = 1$ ($H_x^{(1)} = 2500$ Oe for Permalloy). Notice that $A_1/A_3 = h_x(h_x + 2)/(h_x + 1/2)^2$: for $h_x < 1/4 \to A_1/A_3 < 1$, and for $h_x > 1/4 \to A_1/A_3 > 1$.

(ii) If one studies the magnitude of the oscillatory solutions at $J = 0$, one obtains as solution $|b_{00}^0|^2 = [A_1 \pm \sqrt{A_1^2 - 4A_2}]/(2A_2)$, that exists if $A_1^2 - 4A_2 > 0$. The condition $A_1^2 - 4A_2 = 0$ leads to the condition $(h_x^{(2)})^3 + h_x^{(2)} - 1/2 = 0$ and to $h_x^{(2)} \simeq 0.42$ ($H_x^{(2)} \approx 4200$ Oe for Permalloy).

Notice that the square root in Eq. (29) is imaginary if $J_d(h_x) < J < J_u(h_x)$, with $J_d(h_x) < J_u(h_x) \leqslant J_c(h_x)$:

$$\begin{aligned} J_{u,d} &= (J_c/A_3) \\ &\quad \times[A_1 - 2A_2/A_3 \pm 2\sqrt{(1 - A_1/A_3)A_2 + (A_2/A_3)^2}]. \end{aligned} \tag{31}$$

The ranges of the applied field h_x associated to the existence or not of macrospin solutions of the type of Eq. (28) are (1) $h_x < h_x^{(1)}$. For current densities below J_c in the range $J_u < J < J_c$, there are no solutions that satisfy condition (i). Also $J_d < 0$, meaning that there are no solutions between $0 \leqslant J < J_u$. The static equilibrium state $m_x = 1$ is stable for $0 < J < J_c$. For $J > J_c$, the state $m_x = 1$ becomes unstable, and the macrospin solution (28)–(30) is a stable periodic dynamic solution (a limit cycle), with its oscillation amplitude growing and its frequency diminishing with an increasing applied current density (there is the limiting upper current density $J_c^{(1)}$ already mentioned). Figure 3(a) reflects this case.

(2) $h_x^{(1)} < h_x < h_x^{(2)}$. In the region $J_u < J < J_c$, there are two branches of solutions of the macro spin type (28) corresponding to the $\pm$ signs of Eq. (29) (we will show that the $(-)$ branch is unstable). Here, again $J_d < 0$, so there are no solutions for $0 < J < J_u$. For $J > J_c$, there is only one macrospin solution branch $(+)$, and notice that at $J = J_c$, the amplitude $|b_{00}^0|$ is already finite. For $J < J_c$, the uniform equilibrium state $m_x = 1$ is stable, and becomes unstable for $J > J_c$. Figure 3(b) reflects this case.

(3) $h_x > h_x^{(2)}$. There is a region with $0 < J < J_d$ where there is a real and positive macrospin solution for $|b_{00}^0|^2$, but it is nonphysical since its amplitude of oscillation goes over the upper bound mentioned in (ii), as can be seen in Fig. 3(c). For other current densities, the analysis is the same as for $h_x^{(1)} < h_x < h_x^{(2)}$ (the value of $h_x^{(2)}$ is associated with $J_d = 0$).

In Figs. 3(a)–3(c), we note that when varying the control parameter h_x different types of Hopf bifurcations are seen: when $h_x < 1/4$ the bifurcation is supercritical, and when $h_x > 1/4$ the bifurcation is subcritical [48].

In Fig. 4, we show a comparison between the approximate macrospin solution of Eqs. (28)–(30) and a simulation of the exact macrospin equations written in spherical coordinates, for two different applied fields h_x: the agreement is better for the lower h_x case.

C. Interaction of the uniform auto-oscillation with the nonuniform modes

The auto-oscillation of the macrospin starts over a critical dc current, a problem of interest is to determine its stability with respect to the growth of nonuniform magnetization features.

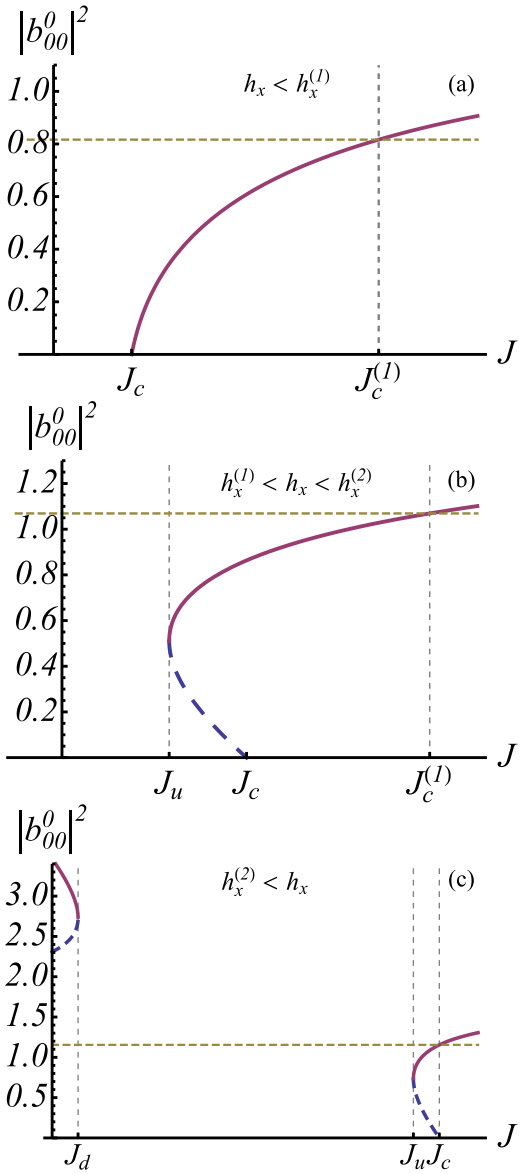

FIG. 3. Amplitude of oscillation of the macrospin mode as a function of the current density from Eq. (29), for different ranges of applied field. (a) $h_x < 1/4$. The graph corresponds to an applied field $h_x = 0.2$. (b) $h_x^{(1)} < h_x < h_x^{(2)}$. The graph corresponds to an applied field $h_x = 0.4$. In the region $J_u < J < J_c$, the branch solutions $\pm$ of Eq. (29) are seen. (c) $h_x > h_x^{(2)}$. The graph corresponds to an applied field $h_x = 0.5$. The horizontal line represents the maximum amplitude that can have the macrospin oscillation, meaning that the solutions close to $J = 0$ are nonphysical.

We do an analytic study of the stability of this uniform auto-oscillation allowing it to attain large amplitudes and studying the onset of exponential growth of nonuniform modes as the dc current density is increased within the range of existence of the auto-oscillation (the following analysis is valid for all the branches of macrospin solutions already discussed). The previously obtained macrospin periodic solution of Eqs. (28)–(30) is

$$a^{\mathrm{ao}} = \rho_{00} b_{00}^0 e^{-i\omega t'} - \nu_{00} b_{00}^{0\,*} e^{i\omega t'}. \tag{32}$$

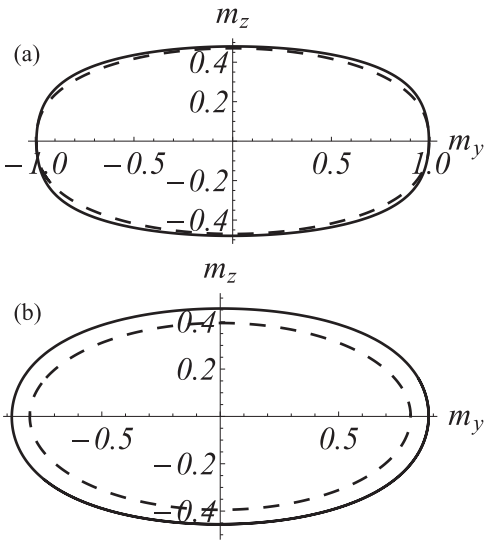

FIG. 4. Comparison between a simulation in spherical coordinates of the macrospin (solid line) and the approximate solution of Eqs. (28)–(30) (dashed line). A projection of the magnetization in the yz plane is shown for a period of oscillation, with (a) $h_x = 0.15$ and $J = 1.1 J_c$, (b) $h_x = 0.25$ and $J = 1.005 J_c$.

Thus we consider a linear perturbation of it:

$$a_{00} = a^{\mathrm{ao}} + \delta a_{00}, \tag{33a}$$

$$a_{mj} = \delta a_{mj}. \tag{33b}$$

Thus, doing an expansion about a^{ao} in Eq. (11a) one gets, the following linear dynamic equation for $\delta \dot{a}_{mj}$ in terms of δa_{mj} and δa^*_{-mj}:

$$i\frac{d\delta a_{mj}}{dt'} \approx \left[\frac{\partial}{\partial a_{mj}}\left(\frac{\partial \mathcal{U}}{\partial a^*_{mj}} + \mathcal{F}_{mj}\right)\right]\Bigg|_{a^{\mathrm{ao}}} \delta a_{mj} + \left[\frac{\partial}{\partial a^*_{-mj}}\left(\frac{\partial \mathcal{U}}{\partial a^*_{mj}} + \mathcal{F}_{mj}\right)\right]\Bigg|_{a^{\mathrm{ao}}} \delta a^*_{-mj}, \tag{34}$$

(given the structure of $\mathcal{U}$ only the terms δa_{mj} and δa^*_{-mj} exist on the right-hand side). The previous equation takes the form:

$$\begin{aligned} i\delta\dot{a}_{mj} &= (A_{mj} + C_{mj}(a^{\mathrm{ao}}))\delta a_{mj} \\ &\quad + [B_{mj} + D_{mj}(a^{\mathrm{ao}})](-1)^m \delta a^*_{-mj} \\ &\quad + i[\beta J - \alpha A_{mj} + E_{mj}(a^{\mathrm{ao}})]\delta a_{mj} \\ &\quad + i[-\alpha B_{mj} + F_{mj}(a^{\mathrm{ao}})](-1)^m \delta a^*_{-mj}, \end{aligned} \tag{35}$$

with the coefficients $A_{mj} - F_{mj}$ given in the Appendix A 1. Doing the change of variables of Eqs. (14)–(17), one obtains from Eq. (35) (and from the analogous form for $\delta \dot{a}^*_{-mj}$) the following equation for $\dot{b}^{(1)}_{mj}$, that couples $b^{(1)}_{mj}$ and $b^{(2)}_{mj}$:

$$\begin{aligned} i\dot{b}^{(1)}_{mj} &= \left[\omega_{mj} b^{(1)}_{mj} - i(\alpha A_{mj} - \beta J) b^{(1)}_{mj} - i\alpha B_{mj}(-1)^m b^{(2)}_{mj}\right] \\ &\quad + [G_{mj}(a^{\mathrm{ao}}) + i H_{mj}(a^{\mathrm{ao}})] b^{(1)}_{mj} \\ &\quad + [I_{mj}(a^{\mathrm{ao}}) + i J_{mj}(a^{\mathrm{ao}})](-1)^m b^{(2)}_{mj}, \end{aligned} \tag{36}$$

with an analogous equation for $\dot{b}^{(2)}_{mj}$. The first term in brackets corresponds to the part without interaction with the macrospin

(already analysed for the linear modes), and the second part includes the interaction with the macrospin via nonlinear terms dependent on its amplitude. The functions G_{mj}, H_{mj}, I_{mj}, and J_{mj} are evaluated at $a^{\rm ao}$ of Eq. (32), and are detailed in Appendix A 2.

Now, based on the linear solution of Eq. (24), the following change of variables is done:

$$b_{mj}^{(1)}(t') = b_{mj}^{0(1)}(t')e^{-i\omega_{mj}t'}e^{-(\alpha A_{mj}-\beta J)t'}, \tag{37}$$

and similarly for $b_{mj}^{(2)}(t')$. Then $\dot{b}_{mj}^{0(1)}(t')$ satisfies the equation

$$\begin{aligned} i\dot{b}_{mj}^{0(1)} =& [G_{mj}(a^{\rm ao}) + i\,H_{mj}(a^{\rm ao})]b_{mj}^{0(1)} \\ &+ [I_{mj}(a^{\rm ao}) + i\,J_{mj}(a^{\rm ao})](-1)^m b_{mj}^{0(2)}e^{2i\omega_{mj}t'} \\ &- i\alpha B_{mj}(-1)^m b_{mj}^{0(2)}e^{2i\omega_{mj}t'}, \end{aligned} \tag{38}$$

and there is a similar equation for $\dot{b}_{mj}^{0(2)}(t')$. We search for a solution in which $b_{mj}^{0(1)}(t')$, $b_{mj}^{0(2)}(t')$ vary slowly in time, thus we can neglect terms of Eq. (38) that have coefficients that vary rapidly [46,47] (terms like $e^{2i\omega t'}$ or $e^{-2i\omega t'}$ for example). Following this idea, we use the constant terms of $G_{mj}(a^{\rm ao})$ and $H_{mj}(a^{\rm ao})$, and the terms proportional to $e^{-2i\omega t'}$ in $I_{mj}(a^{\rm ao})$ and $J_{mj}(a^{\rm ao})$, and we obtain the following approximate equation for $b_{mj}^{0(1)}$, $b_{mj}^{0(2)}$:

$$\begin{aligned} i\dot{b}_{mj}^{0(1)} =& (G'_{mj} + i\,H'_{mj})\left|b_{00}^0\right|^2 b_{mj}^{0(1)} \\ &+ (I'_{mj} + i\,J'_{mj}){b_{00}^0}^2(-1)^m b_{mj}^{0(2)}e^{2i(\omega_{mj}-\omega)t'}, \end{aligned} \tag{39}$$

with the expressions for $G'_{mj} - J'_{mj}$ given in Appendix A 3 (there is a similar equation for $\dot{b}_{mj}^{0(2)}$).

The solution to the system of equations for $b_{mj}^{0(1)}$, $b_{mj}^{0(2)}$ is

$$b_{mj}^{0(1)} = u_{mj}^0 e^{i(\omega_{mj}-\omega)t'}e^{\gamma_{mj}t'}, \tag{40}$$

with

$$\begin{aligned} \gamma_{mj} =& \pm\sqrt{(|I'_{mj}|^2 + |J'_{mj}|^2)\left|b_{00}^0\right|^4 - \left(\omega_{mj} - \omega + G'_{mj}\left|b_{00}^0\right|^2\right)^2} \\ &+ H'_{mj}\left|b_{00}^0\right|^2. \end{aligned} \tag{41}$$

Since we are looking for instabilities, we take the (+) sign in the previous solution, and the solution for the mode $b_{mj}^{(1)}$ takes the form

$$\begin{aligned} b_{mj}^{(1)}(t') =& u_{mj}^0 e^{i(\omega_{mj}-\omega)t'}e^{\gamma_{mj}t'}e^{-i\omega_{mj}t'}e^{-(\alpha A_{mj}-\beta J)t'}, \\ =& u_{mj}^0 e^{-i\omega t'}e^{\gamma_{mj}t'-(\alpha A_{mj}-\beta J)t'}, \end{aligned} \tag{42}$$

i.e., it oscillates with the same frequency ω as the macrospin. Then, the mode $b_{mj}^{(1)}$ will have an exponential growth if $\gamma_{mj} > \alpha A_{mj} - \beta J$, or

$$\begin{aligned} &\sqrt{\left({I'_{mj}}^2 + {J'_{mj}}^2\right)\left|b_{00}^0\right|^4 - \left(\omega_{mj} - \omega + G'_{mj}\left|b_{00}^0\right|^2\right)^2} \\ &\quad > \alpha A_{mj} - \beta J - H'_{mj}\left|b_{00}^0\right|^2, \end{aligned} \tag{43}$$

a condition that will be analyzed in the following.

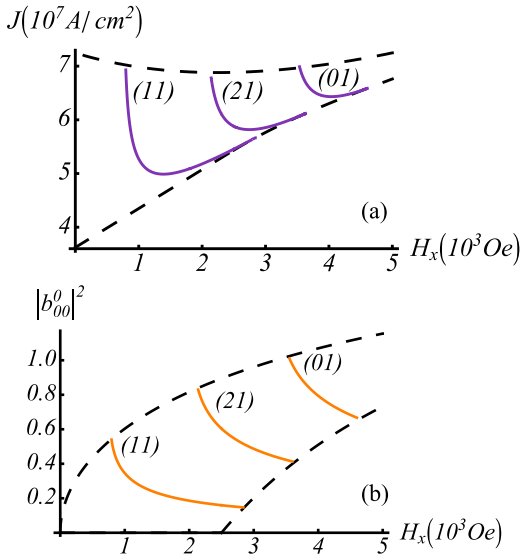

FIG. 5. (a) Graph of the threshold current density at which nonuniformities of the magnetization start growing. The three curves correspond to the first three modes to grow exponentially [(11),(21), and (01)]. The lower segmented line corresponds to the current at which the uniform mode starts auto-oscillation and the upper segmented line corresponds to $J_c^{(1)}$. (b) Graph of the threshold amplitude attained by the macrospin when the nonuniformities of the magnetization start (first three nonuniform modes). The lower segmented line corresponds to the minimum amplitude of oscillation and the upper segmented line is associated with the maximum amplitude possible.

IV. APPLICATIONS OF THE SIMPLER MODEL, NUMERICAL RESULTS

In the following, we will show applications of the theoretical model and present some numerical results. For all the plots that follow we will consider that the free layer is made of Permalloy, with the following associated parameters: $4\pi M_s = 10^4$ Oe, $l_{\rm ex} = 5.7$ nm, $\epsilon = 0.17$, and $\alpha = 0.01$.

A. Instabilities, examining theoretical results

The expression of Eq. (43) that establishes possible linear exponential growth of nonuniform modes depends on the current and magnetic field applied to the system. Thus, for a given applied magnetic field, by solving the equality on Eq. (43) a threshold dc current $J_t^{(mj)}$ can be found at which the nonuniform mode (m, j) destabilizes. Figure 5(a) shows J_t for the three first nonuniform modes that go unstable. In Fig. 5(b), we graph the amplitude that the macrospin has at the point where the first three nonuniform magnetization modes grow exponentially in this linear analysis. Notice that we graph three nonuniform modes since there is evidence in some systems [49–52] that these modes may stabilize via nonlinear terms and coexist with an adjusted uniform mode.

Also, with Eq. (43) one can establish if the different branches of the macrospin solutions that were found [Eqs. (28)–(30)] are stable or not with respect to uniform perturbations. This can be done evaluating Eq. (43) for

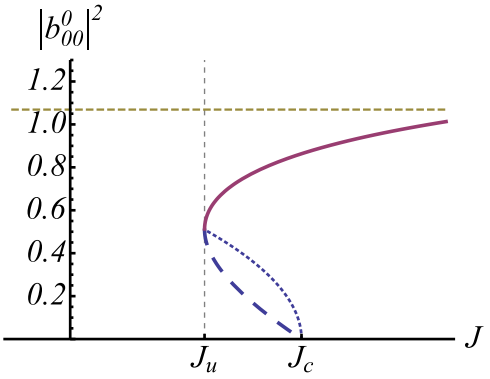

FIG. 6. Plot of the (±) branch solutions of Eq. (29) for the amplitude squared of the macrospin periodic solutions of Eq. (28) [(+), corresponds to the continuous line, and (−) to the segmented line]. The dotted line is the instability line of Eq. (45).

$(m, j) = (0,0)$, and it simplifies to

$$|J'_{00}||b_{00}^0|^2 > \alpha A_{00} - \beta J - H'_{00}|b_{00}^0|^2, \tag{44}$$

which gives an instability condition as follows:

$$|b_{00}^0|^2 < \sqrt{\frac{1 - J/J_c}{A_2}}. \tag{45}$$

As discussed in Sec. III B for $h_x > 1/4$ there are two branches of macrospin solutions of the type of Eq. (28). In Fig. 6, the latter limit curve of Eq. (45) is plotted and shows that the lower (−) branch is unstable to uniform perturbations, while the upper one (+) is stable. For $h_x < 1/4$, the only branch for $J > J_c$ is stable to uniform perturbations.

It is to be noted that since for $h_x > 1/4$ the (+) branch is stable and occurs at a gap in amplitude with respect to the equilibrium uniform state: thus in Fig. 5(b), that plots the amplitudes at instability of the nonuniform modes, one sees a lower segmented curve for the allowed values of $|b_{00}^0|^2$. The upper segmented curve is associated with the upper bound mentioned in Sec. III B. From Fig. 5(a) one infers that for $h_x > 1/4$ a very small change of current density leads to the nonuniform modes becoming unstable, and this is occurring with an associated significant increase in amplitude of oscillation [Fig. 5(b)]. Also, for fields higher than $h_x \simeq 0.28$ the first nonuniform mode is always unstable. The previous comment plus the high sensitivity to changes in current density of Fig. 5(a) show that a practical limiting applied field for stability of the uniform auto-oscillation is approximately $h_x = 1/4$, or $H_x = \pi M_s$.

Also, Fig. 6 shows the coexistence of two stable solutions [the static equilibrium and the (+) branch] when the current lies in the interval $J_u < J < J_c$, this occurs for $h_x > 1/4$. To first order in $|b_{00}^0|^2$, the difference in energy (averaged over time) between the macrospin solution of the upper branch and the static uniform solution is $4\pi M_s^2 V \omega |b_{00}^0|^2$: this means that for a field slightly over $h_x = 1/4$, and for a disk of a radius of 50 nm., this difference in energy may be much greater than the thermal energy $k_B T$, with T an ambient temperature. Thus, for currents below the critical current J_c, there is range of fields over $h_x = 1/4$ where there is bistability in the system between a periodic macrospin solution and the uniform static solution (only for fields very close to $h_x = 1/4$, one would see thermal switching between these two states).

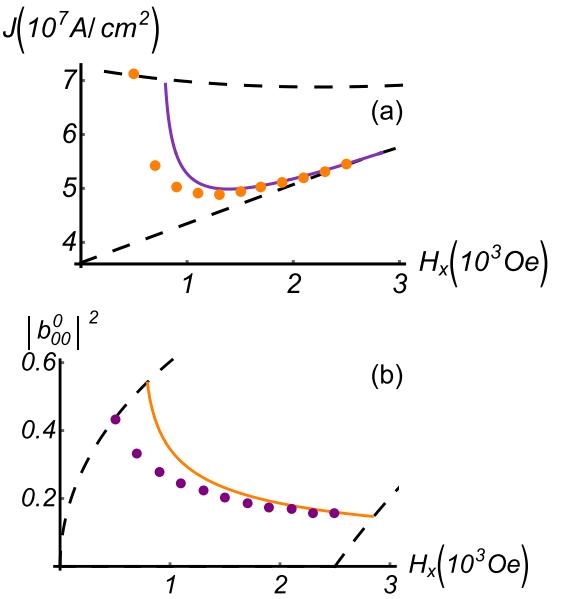

FIG. 7. (a) Comparison of the theoretical and numerical threshold current densities for the growth of the first nonuniform mode: points are numerical data, and the curve the theoretical prediction of Eq. (43). (b) Comparison of the theoretical and numerical threshold oscillation amplitude for the growth of the first nonuniform mode. The segmented curves have the same significance as those equivalent curves of Figs. 5(a) and 5(b).

B. Instabilities, comparison with numerical simulations

The previous theoretical analysis of Sec. III C on the instability of the macrospin due to growth of nonuniform modes made use of some approximations like approximating the exchange energy and the exclusion of nonresonant terms. The objective of this section is to compare those approximate theoretical results with numerical simulations that address the growth of these nonuniform modes without using approximations of the underlying equations. Thus a system of three coupled equations is studied numerically: one is Eq. (25) that describes the exact dynamics of the macrospin (if uncoupled), the others are the linearized equation (35) for $\delta\dot{a}_{mj}$ when the macrospin amplitude $a_{00} = a^{ao}$ has attained a large value, and a similar one for $\delta\dot{a}^*_{-mj}$ that follows from Eq. (35).

In order to find a numerical instability, we proceed by solving the macrospin equation (25) as a function of a slowly increasing dc current density $J = J(t')$ (in this way we are in an adiabatically changing stationary periodic solution, and we are also neglecting the influence of other modes on the macrospin), and then with this macrospin solution we numerically solve the mentioned equations for δa_{mj} and δa^*_{-mj}. At the moment $t' = \tau$ in which we evidence an unstable growth of the nonuniform modes amplitudes, we establish as $J(\tau)$ the threshold current density for instability of the macrospin.

The following Fig. 7(a) shows a comparison between the theoretical prediction for the current density threshold for the growth of the first nonuniform mode versus the analogous

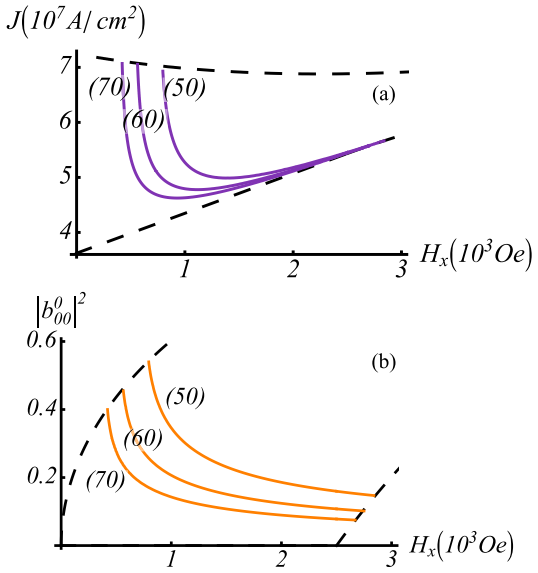

FIG. 8. The solid curves represent, for different radii: $R = \{50\text{ nm}, 60\text{ nm}, 70\text{ nm}\}$: (a) the threshold current density that must be applied in order to start observing nonuniformities of the magnetization in the free layer and (b) the threshold oscillation amplitude that are attained by the macrospin when nonuniformities of the magnetization start in the free layer. All the curves correspond to the growth of the first nonuniform mode ($m = j = 1$). The segmented curves have the same significance as those equivalent curves of Figs. 5(a) and 5(b).

threshold obtained numerically: we see a similar behavior between the numerical (in principle exact) and theoretical (approximate) thresholds, with the numerical threshold being lower. Figure 7(b) shows a comparison between the theoretical prediction for the amplitude of oscillation threshold for the growth of the first nonuniform mode, versus the analogous threshold obtained numerically.

C. Instabilities, dependence with size

In this section we study the dependence of the instability of the first nonuniform mode ($m = j = 1$) on the radius of the disk, by maintaining its thickness constant at $h = 5$ nm. In particular, the radii considered are $R = \{50\text{ nm}, 60\text{ nm}, 70\text{ nm}\}$, and we use parameters for Permalloy. The results are presented in Figs. 8(a) and 8(b). In Fig. 8(a), it is seen that the smaller the radius of the disk, the larger is the threshold dc current density needed to de-stabilize the first nonuniform mode. While in Fig. 8(b) it is seen that the smaller the radius of the disk, the bigger the amplitude of oscillation of the uniform mode that is reached when the nonuniformities appear [the limiting segmented curves of Figs. 8(a) and 8(b) have the same significance as those equivalent curves of Figs. 5(a) and 5(b)].

The dependence of the instability of the macrospin on the disk's size, or more specifically its radius, in this model comes through the exchange field. As can be seen from Eq. (12), $\mathcal{U}_{\text{ex}} \propto (l_{\text{ex}}/R)^2 |a_{mj}|^2$, meaning that smaller radii effectively increase the energy of non-uniform modes relative to the uniform one, meaning the latter is more stable at smaller radii. This is consistent with the idea that uniform magnetization configurations are stabilized in samples of smaller sizes.

V. A DISK WITH EDGE EFFECTS, EXACT DEMAGNETIZING FIELD

The disk dynamics changes if one goes beyond the previous model in which the demagnetizing field was approximated by its main term $-4\pi M_z \hat{z}$, or the very flat thin film limit. In the following, we will consider the effect of the full demagnetizing field, which introduces important edge effects: the smaller the radius the more relevant these become. Notice that the full demagnetizing field has contributions from surface charges as well as volume charges. These new terms of the demagnetizing field are proportional to the thickness h of the film, which in this model is considered small. In the Appendix, we detail the calculation of the different terms that contribute to the averaged demagnetizing field over the thickness of the disk. The calculation proceeds by determining the magnetostatic potential via its integral representation in terms of surface and volume charges, with the appropriate Green's function written in terms of an integral representation that involves Bessel functions, Eq. (B2). We do not explicitly separate static and dynamic components of the magnetization in the calculations of demagnetizing fields presented in the Appendix.

In Ref. [53], the demagnetizing fields of uniform magnetization configurations in nonellipsoidal samples were calculated. Previous studies have calculated demagnetizing fields in ferromagnetic very thin circular dots magnetized in plane, with the aim to determine the spin wave modes of these dots. We mention Ref. [54] where demagnetizing fields have been calculated in an equivalent way through use of volume integral representations: tensorial Green's functions are used averaged over the thickness of the dot, and the fields are calculated within a basis that diagonalizes the exchange operator (it is a similar basis to the one used in this work, i.e., written in terms of Bessel functions); dynamic and static contributions of the dipolar fields are separated, the equilibrium magnetization is considered uniform and the eigenvalue problem for the frequencies in their basis is simplified by neglecting nondiagonal terms. Also Refs. [55,56] present an approximate variational method to determine the modes of very thin circular ferromagnetic dots: they calculate demagnetizing fields via the same tensorial Green's functions averaged over the thickness of the dot, and indeed use the integral representation of the basic kernel in terms of Bessel functions, i.e., Eq. (B2); they approximate the equilibrium configuration as uniform, use approximate forms of the dynamic demagnetizing fields, introduce a model for dipolar pinning, and they do variational calculations within restricted trial sets.

A. Equilibrium configuration

With the demagnetizing field in its full form the equilibrium magnetization is no longer fully aligned as $\vec{m} = \hat{x}$. In order to calculate the equilibrium configuration, i.e., a^{eq}_{mj}, we need to impose

$$\left.\frac{\partial \mathcal{U}}{\partial a^*_{mj}}\right|_{eq} = 0 \tag{46}$$

with $\mathcal{U}$ now including the full demagnetizing energy $\mathcal{U}_D$, which is given in Eqs. (B5)–(B13) of the Appendix. The previous system of nonlinear equations, Eqs. (46), was solved using an

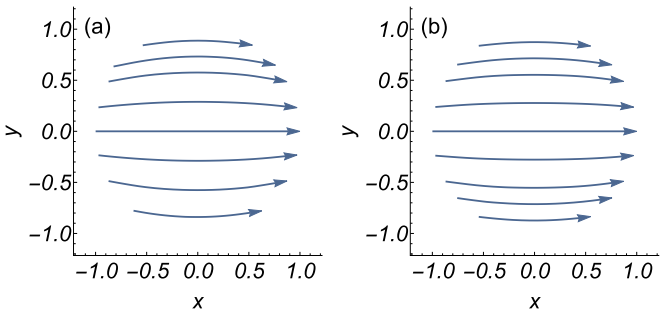

FIG. 9. Magnetization orientation in minimum energy configurations of the disk: (a) $h_x = 0.1$ and (b) 0.2. In both cases, the magnetization is in plane, i.e., $m_z = 0$.

iterative method, that is, an extension of the Newton-Raphson method [57,58]. Initially, one solves for the linear corrections of the equilibrium, and then this solution is used as a first seed of an iterative process that converges to the nonlinear solution. We find that the $a^{\rm eq}_{mj}$ are real, that $a^{\rm eq}_{mj} = 0$ if m is odd, and that $a^{\rm eq}_{mj} \neq 0$ if m is even. Also, $a^{\rm eq}_{-mj} = -(-1)^m a^{\rm eq}_{mj}$, leading to $m_z = 0$.

In Fig. 9, two equilibrium configurations are shown for two different applied fields. They correspond to an almost aligned magnetization configuration with some curvature that mimics a bit the circular geometry of the disk: it occurs in order to minimize magnetic surface charges on the edges of the disk, and consequently the full energy of the system.

Notice that depending on the dimensions of the free layer, it is known that the minimum energy configuration may be either a vortex state or an almost saturated state in the plane or out of the plane [59,60]. The dimensions used in this work, i.e., $R = 50$ nm and $h = 5$ nm only allow an equilibrium magnetization almost saturated in the plane.

B. Linear dynamics

The linear magnetization dynamics in thin circular disks has been studied in cases where the magnetizaton equilibrium configuration corresponds to a vortex [61–64], or in a case of almost saturation in plane [65]. There is a large difference between the spatial profiles of the modes corresponding to the previous two cases of equilibrium configurations with vortices or quasisaturated states. The basis of Eq. (7) that we use to describe the dynamics of the magnetization would describe better the case of a vortex equilibrium configuration when both the geometry and the magnetization state have circular symmetry, but in our case of magnetization almost saturated in plane in the direction of the applied magnetic field this basis is still practical since it assures satisfying the boundary conditions in the circular geometry although the magnetization state breaks the circular symmetry.

In order to study the linear dynamics in the case of full consideration of the demagnetizing field, the dynamic equations without dissipation (11a) are approximated to linear order by writing $a_{mj} = a^{\rm eq}_{mj} + \tilde{a}_{mj}$:

$$i\dot{\tilde{a}}_{mj} = \sum_{m'j'} \left(A^{m'j'}_{mj}\tilde{a}_{m'j'} + B^{m'j'}_{mj}\tilde{a}^*_{m'j'}\right), \tag{47}$$

where $A^{m'j'}_{mj} = \partial^2\mathcal{U}/\partial a_{m'j'}\partial a^*_{mj}|_{eq}$ and $B^{m'j'}_{mj} = \partial^2\mathcal{U}/\partial a^*_{m'j'}\partial a^*_{mj}|_{eq}$. Or using matrices, schematically:

$$i\frac{d}{dt'}\begin{pmatrix}\tilde{a}_{mj}\\ \tilde{a}^*_{mj}\end{pmatrix} = \begin{pmatrix}A^{m'j'}_{mj} & B^{m'j'}_{mj}\\ -B^{m'j'*}_{mj} & -A^{m'j'*}_{mj}\end{pmatrix}\begin{pmatrix}\tilde{a}_{m'j'}\\ \tilde{a}^*_{m'j'}\end{pmatrix} = \mathbf{M}_1\begin{pmatrix}\tilde{a}_{m'j'}\\ \tilde{a}^*_{m'j'}\end{pmatrix}. \tag{48}$$

The matrix $\mathbf{M}_1$ is diagonalizable through the following Bogoliubov type transformation:

$$\tilde{a}_{mj} = \sum_n \left(\lambda^n_{mj}b_n - \mu^n_{mj}b^*_n\right), \tag{49}$$

or using matrices (compact notation):

$$\begin{pmatrix}\tilde{a}_{mj}\\ \tilde{a}^*_{mj}\end{pmatrix} = \begin{pmatrix}\lambda^{n'}_{mj} & -\mu^{n'}_{mj}\\ -\mu^{n'*}_{mj} & \lambda^{n'*}_{mj}\end{pmatrix}\begin{pmatrix}b_{n'}\\ b^*_{n'}\end{pmatrix} = \mathbf{M}_2\begin{pmatrix}b_{n'}\\ b^*_{n'}\end{pmatrix} = \sum_{n'}\left\{b_{n'}\begin{pmatrix}\lambda^{n'}_{mj}\\ -\mu^{n'*}_{mj}\end{pmatrix} + b^*_{n'}\begin{pmatrix}-\mu^{n'}_{mj}\\ \lambda^{n'*}_{mj}\end{pmatrix}\right\}. \tag{50}$$

The equation for the new variables b_n, b^*_n becomes

$$i\frac{d}{dt}\begin{pmatrix}b_n\\ b^*_n\end{pmatrix} = \mathbf{M}_2^{-1}\mathbf{M}_1\mathbf{M}_2\begin{pmatrix}b_{n'}\\ b^*_{n'}\end{pmatrix} = \mathbf{D}\begin{pmatrix}b_{n'}\\ b^*_{n'}\end{pmatrix}, \tag{51}$$

where $\mathbf{D} = \mathbf{M}_2^{-1}\mathbf{M}_1\mathbf{M}_2$ is a diagonal matrix. Also, in order for the transformation (50) to be canonical, the following needs to be satisfied:

$$\sum_{mj}\left(\lambda^n_{mj}{}^*\lambda^{n'}_{mj} - \mu^n_{mj}\mu^{n'}_{mj}{}^*\right) = \delta^n_{n'}, \tag{52a}$$

$$\sum_{mj}\left(\lambda^n_{mj}{}^*\mu^{n'}_{mj} - \mu^n_{mj}\lambda^{n'}_{mj}{}^*\right) = 0. \tag{52b}$$

The diagonal terms of the matrix $\mathbf{D}$ are the eigenfrequencies of oscillation, ω_n, of the different modes, i.e., in this linear approximation $b_n = b^0_n e^{-i\omega_n t'}$ are independent oscillators.

In order to analyze how the frequencies of the modes are modified as one considers the effect of the full demagnetizing field, we write this field as (averaged over the thickness of the disk):

$$\vec{H}_D = -4\pi M_z(\rho,\phi)\hat{z} + \epsilon\left[h^z_D(M_z)\hat{z} + \vec{h}^{\perp}_D(M_\perp)\right]. \tag{53}$$

A control parameter ϵ has been introduced that is equal to zero when the demagnetizing field is approximated by its very thin film limit, and it is equal to one when the full demagnetizing field is considered. Recourse to this control parameter allows to follow the evolution of the linear modes of the disk from the analytical form found in the very thin film limit approximation [Eqs. (14)–(18b)] to their more complex form as the finite transverse dimensions and small but finite thickness of the film is considered: effectively increasing this control parameter is equivalent to artificially increasing the thickness of the disk.

In Fig. 10(a), we show the evolution of the frequencies of the first modes of the disk as the control parameter ϵ increases, for an applied magnetic field $h_x = 0.1$. The lower blue points

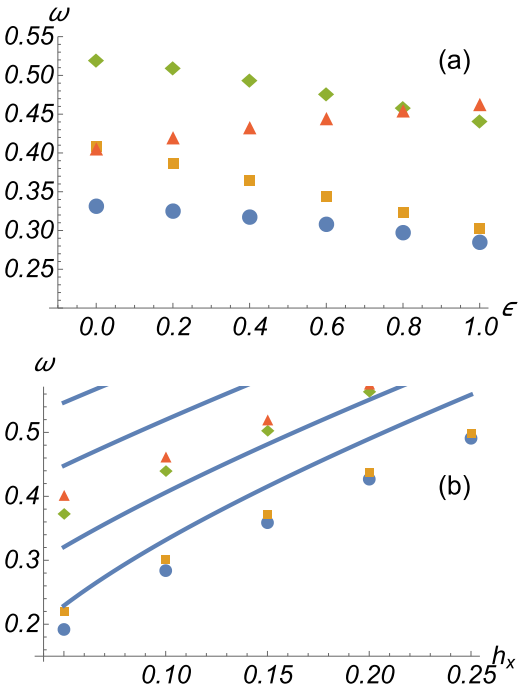

FIG. 10. (a) Variation of the frequencies of the lowest modes with changing control parameter ϵ, for $h_x = 0.1$. Blue circular points represent the evolution of the mode $(m = 0, j = 0)$, that corresponds to mode $n = 1$ in (b). The orange squares and red triangles represent the evolution of modes $(m = 1, j = 1)^{(1,2)}$, that become modes $n = 2$ and $n = 4$ respectively in (b). The green rhombi represent the evolution of one of the modes $(m = 2, j = 1)^{(1,2)}$, which becomes mode $n = 3$ in (b). (b) Variation of the frequencies of the lowest modes with changing applied magnetic field: lines correspond to frequencies at $\epsilon = 0$, shown in Fig. 2, points to the case $\epsilon = 1$, with corresponding colors to adjacent figure (a).

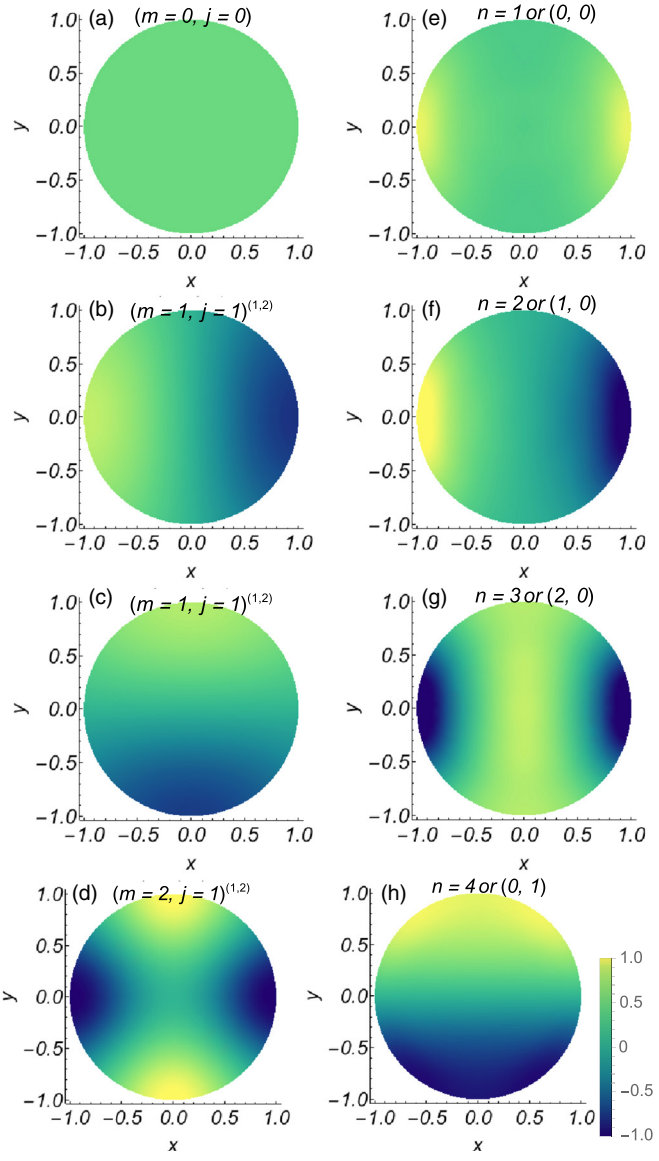

FIG. 11. Graphic representation of the first four lowest modes in the disk, with an applied magnetic field of $h_x = 0.1$. The colors represent the values of the m_z component of the dynamic magnetization of each mode. The figures to the left represent the lowest modes at $\epsilon = 0$ and those to the right those for $\epsilon = 1$: they are ordered from lower to higher frequencies (labels for the modes in the $\epsilon = 0$ and $\epsilon = 1$ cases are explained in the text).

correspond to the evolution of the frequency of the original mode $(m, j) = (0,0)$, which represents the macrospin at $\epsilon = 0$: it diminishes its frequency with increasing strength of the "extra" demagnetizing field. The orange/red points represent the initially degenerate $(m, j)^{(1,2)} = (1,1)^{(1,2)}$ modes: they mix and the frequencies do separate and increase/decrease with an increasing effective thickness of the disk (these modes at $\epsilon = 0$ correspond to nonzero values of a_{11}, a^*_{-11} and their complex conjugates). The green points correspond to the evolution of the frequencies of a mode that corresponds to a mixture of $(m, j)^{(1,2)} = (2,1)^{(1,2)}$ modes at $\epsilon = 0$, its frequency diminishes with full consideration of demagnetizing effects. Also, Fig. 10(b) shows the dependence of the frequencies of the first modes on the applied magnetic field: they increase monotonically with it (full curves correspond to $\epsilon = 0$ modes, and points to the lowest modes at $\epsilon = 1$, with corresponding colors to the previous figure).

In the following Fig. 11, we plot the shapes of different linear modes of the thin disk. For a given mode (n), with associated nonnull b_n and b^*_n, from Eq. (49) one determines the associated $\tilde{a}_{mj}$, i.e., as $\tilde{a}_{mj} = b^0_n(\lambda^n_{mj} - \mu^n_{mj})$ if one chooses $b_n = b^0_n$ real (this amounts to choosing an origin of time). Then, from Eq. (7), one may determine $a(\vec{x},t)$ associated to mode (n). Furthermore, in solving the eigenvalue problem involved in Eq. (51), we numerically found that there are modes with $\lambda^n_{-mj} = (-1)^m\lambda_{mj}$ and $\mu^n_{-mj} = (-1)^m\mu_{mj}$, or $\lambda^n_{-mj} = -(-1)^m\lambda_{mj}$ and $\mu^n_{-mj} = -(-1)^m\mu_{mj}$. In the first case, we find

$$\begin{aligned} m_z &= \sqrt{2}\mathrm{Re}(a) \\ &= \sqrt{2}b^0_n \sum_j N_{0j}\left(\lambda^n_{0j} - \mu^n_{0j}\right) J_0(\kappa_{0j}\rho)\cos(\omega_n t) \\ &+ 2\sqrt{2}b^0_n \sum_{m>0 j} N_{mj} J_m(\kappa_{mj}\rho)\left(\lambda^n_{mj} - \mu^n_{mj}\right) \\ &\times \cos m\phi \cos(\omega_n t), \end{aligned} \tag{54}$$

$$
\begin{aligned}
m_y &= \sqrt{2}\mathrm{Im}(a) \\
&= -\sqrt{2}b_n^0 \sum_j N_{0j}(\lambda_{0j}^n + \mu_{0j}^n) J_0(\kappa_{0j}\rho)\sin(\omega_n t) \\
&\quad - 2\sqrt{2}b_n^0 \sum_{m>0 j} N_{mj} J_m(\kappa_{mj}\rho)\left(\lambda_{mj}^n + \mu_{mj}^n\right)\cos m\phi \sin(\omega_n t),
\end{aligned}
\tag{55}
$$

i.e., these are stationary modes that have reflection symmetry with respect to the x axis (symmetry with respect to $\phi \to -\phi$). And in the second case, we find

$$
\begin{aligned}
m_z &= \sqrt{2}\mathrm{Re}(a) \\
&= 2\sqrt{2}b_n^0 \sum_{m>0 j} N_{mj} J_m(\kappa_{mj}\rho)\left(\lambda_{mj}^n + \mu_{mj}^n\right)\sin m\phi \sin(\omega_n t),
\end{aligned}
\tag{56}
$$

$$
\begin{aligned}
m_y &= \sqrt{2}\mathrm{Im}(a) \\
&= 2\sqrt{2}b_n^0 \sum_{m>0 j} N_{mj} J_m(\kappa_{mj}\rho)\left(\lambda_{mj}^n - \mu_{mj}^n\right)\sin m\phi \cos(\omega_n t),
\end{aligned}
\tag{57}
$$

i.e., these modes are stationary antisymmetric with respect to reflections with respect to the x axis (antisymmetry with respect to $\phi \to -\phi$).

Also, it is to be noted that the modes separate into those that have m even and m odd (the second condition only arises if $\lambda_{0j}^n = 0$ and $\mu_{0j}^n = 0$), and this leads to antisymmetric or symmetric modes with respect to reflections with respect to the y axis, which depends on them being proportional to $\cos(m\phi)$ or to $\sin(m\phi)$.

Thus we get the result that taking into account the full demagnetizing field, the modes no longer circulate as in the simpler version of the model, but instead they are stationary modes with definite symmetries with respect to the x and y axis, and this will be seen in the following figures. This may be attributed to the magnetic charges introduced by aligning the magnetization along the x axis, then the differential equations for the modes are space dependent and reflect that the x and y axis are symmetry axes.

In Fig. 11, we have plotted over the disk the quantity $\mathrm{Re}(\tilde{a}) = m_z/\sqrt{2}$ (at $t = 0$ and assuming b_n to be real), thus it is basically the m_z of the dynamic magnetization, and it is assumed to be in the range $[-1,1]$ (this is arbitrary since these are linear modes). The applied magnetic field is taken as $h_x = 0.1$. The left column of Fig. 11 shows the shape of the four lowest frequency modes in the limit $\epsilon \to 0$ (notice that particular linear combinations of the modes of the simpler model that rotate in different directions give rise to these modes). The first corresponds to the macrospin mode [Fig. 11(a)], which shows a uniform value as expected, it corresponds to the mode $(m,j) = (0,0)$ in the notation introduced in the simpler model. Figures 11(b) and 11(c) are associated to linear combinations of the degenerate modes $(m,j)^{(1,2)} = (1,1)^{(1,2)}$, and Fig. 11(d) corresponds to a linear combinations of the modes $(m,j) = (2,1)$. The right column of Fig. 11 shows the four modes with lowest frequencies when $\epsilon = 1$, occurring at 7.98 GHz, 8.38 GHz, 12.35 GHz, and 12.96 GHz, respectively. In general, as $\epsilon \to 1$, there is more localization of the modes at the edges in the regions where $y \simeq 0$, where the magnetic charges are stronger. In the case of the macrospin mode, it gets curved close to the edges attaining higher amplitude there while maintaining an almost uniform value in the interior (the variable a_{00} is dominant). Figure 11(f) has as as dominant variables a_{11} and $a_{-1,1}$. And Figs. 11(g) and 11(h) have as dominant variables a_{21}, $a_{-2,1}$ and a_{11}, $a_{-1,1}$, respectively.

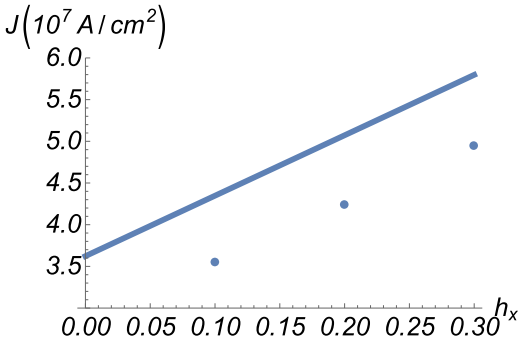

FIG. 12. The points correspond to the critical current densities of the lowest mode as a function of the applied magnetic field for $\epsilon = 1$, or full demagnetizing field. The continuous line corresponds to the macrospin critical current density at $\epsilon = 0$, or the very thin disk limit.

The previous modes may be named through the classification used for modes in rectangular dots, that depends on nodal lines. The first, Fig. 11(e), may be named (0,0) or fundamental (mode with no nodes); the second, Fig. 11(f), as (1,0) or 1-backward mode (a mode with one nodal plane perpendicular to the in-plane magnetization); the third, Fig. 11(g), as (2,0) or 2-backward mode (a mode with two nodal plane perpendicular to the in-plane magnetization); and the fourth, Fig. 11(h), as (0,1) or 1-Damon-Eshbach mode (a mode with one nodal plane parallel to the in-plane magnetization).

It is important to note that our results for $\epsilon = 1$ coincide very well with those of micromagnetic simulations done in Ref. [30], both in the values of the frequencies of the modes as well as in their shapes (there are small differences that may be attributed to slightly different values for the saturation magnetization and the exchange constant).

Next, we study the effect of an applied current to linear order, considering the associated spin transfer torque and dissipation:

$$
i\dot{\tilde{a}}_{mj} \approx (1 - i\alpha)\sum_{m'j'}\left(A_{mj}^{m'j'}\tilde{a}_{m'j'} + B_{mj}^{m'j'}\tilde{a}_{m'j'}^*\right) + i\beta J\tilde{a}_{mj}.
\tag{58}
$$

In terms of the b_n variables of Eq. (50), these previous equations read

$$
i\frac{d}{dt}\begin{pmatrix} b_n \\ b_n^* \end{pmatrix} = \mathbf{D}\begin{pmatrix} b_{n'} \\ b_{n'}^* \end{pmatrix} + i\mathbf{M}_3\begin{pmatrix} b_{n'} \\ b_{n'}^* \end{pmatrix}.
\tag{59}
$$

We approximate the induced nonoscillatory behavior of modes n considering the diagonal terms of matrix $\mathbf{M}_3$, i.e., $b_n \simeq b_n^0 e^{(-i\omega_n + \gamma_n)t'}$. For each applied magnetic field, a critical current density may be found such that $\gamma_n = 0$. In Fig. 12, the critical current density for the second mode is shown (this mode has

the lowest critical current), and a comparison is made with the critical current density of the macrospin, i.e., $J = \alpha(h_x + 1/2)/\beta$ for the macrospin. Thus precessions may be observed at current densities that are lower than that predicted for the uniform macrospin model. In Ref. [66], normal modes are excited via spin transfer torque: they show that the first excited mode corresponds to the lowest frequency, but in our case it happens for the mode of the second lowest frequency, this may occur since we use a lower applied field than them.

C. Mode with lowest critical current, its excitation and instability

The modes we labeled as 1,2 (b_1,b_2) have the lowest frequencies, and these are quite similar, with b_1 the quasiuniform mode and the one with lowest frequency. Also their critical currents are similar, $J_1^{\rm crit} \sim J_2^{\rm crit}$. However, the mode b_2 has the lowest critical current (the critical current density not only depends directly on the frequency), it will auto-oscillate first as one increases the current density.

We will study the range of applied currents in which the mode b_2 auto-oscillates, and determine its linear stability range with respect to other modes becoming unstable: we will compare theoretical predictions with numerical results.

If we apply a current density $J > J_2^{\rm crit}$, the mode b_2 starts to auto-oscillate, we write an equation for its nonlinear growth assuming the other modes have very low amplitudes. The dynamic equations for the modes b_n,b_n^* are

$$i\frac{d}{dt}\begin{pmatrix} b_n \\ b_n^* \end{pmatrix} = \mathbf{M}_2^{-1} i\frac{d}{dt}\begin{pmatrix} \tilde{a}_{mj} \\ \tilde{a}_{mj}^* \end{pmatrix}. \tag{60}$$

Considering that only mode b_n dominates the previous dynamics, and that one only keeps resonant terms up to order 3 without interaction between modes, one obtains the following approximate equation for the time evolution of b_n:

$$i\frac{db_n}{dt'} = C_n^1 b_n + C_n^2 |b_n|^2 b_n. \tag{61}$$

We look for an auto-oscillatory solution to the previous equation for mode b_2, i.e., $b_2 = b_2^0 e^{-i\omega_2 t'}$, with a real frequency ω_2. Imposing this, one obtains that

$$\omega_2 = Re\left(C_2^1 + C_2^2 |b_2^0|^2\right), \tag{62a}$$

$$Im\left(C_2^1 + C_2^2 |b_2^0|^2\right) = 0. \tag{62b}$$

Thus one obtains an expression for the frequency of auto-oscillation ω_2 that depends on the amplitude of oscillation $|b_2^0|$ and an expression for this latter amplitude as a function of the applied current density and applied magnetic field. In Fig. 13, we show a comparison between this previous theoretical prediction for this amplitude of auto-oscillation versus numerical results for it, they reasonably agree (in the numerical solution one changes adiabatically the applied current). The cloud of blue points that is observed in the numerical solution is explained since in the latter solution for b_2 not only the resonant terms shown in Eq. (61) are included, but the nonresonant terms also. In this way, the general solution for this variable is of the form: $b_2 = b_2^0 e^{-i\omega_2 t'} + b_2^1 e^{-2i\omega_2 t'} + b_2^2 e^{-3i\omega_2 t'} + \ldots$. When its magnitude is plotted, an oscillatory part follows, that explains the blue cloud of points.

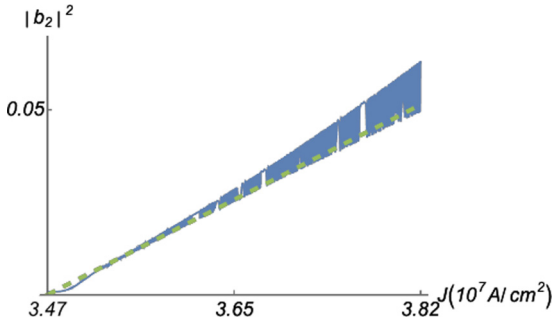

FIG. 13. Comparison between the theoretical prediction (dashed green line) and numerical result (blue) for the amplitude of auto-oscillation of mode b_2, considering an applied magnetic field $h_x = 0.1$.

Now we study theoretically the linear stability of the previous auto-oscillatory solution for the mode b_2. Thus we assume a solution with linear perturbations as follows:

$$b_2 = b_2^0 e^{-i\omega_2 t'} + \delta b_2, \tag{63a}$$

$$b_j = \delta b_j. \tag{63b}$$

The form that takes the equation for mode j, considering that mode b_2 is auto-oscillating, is the following:

$$i\frac{d\delta b_j}{dt'} = C_1 \delta b_j + C_2 \delta b_j^* + C_3(b_2)\delta b_j + C_4(b_2)\delta b_j^*. \tag{64}$$

We search for solutions of the form $\delta b_j = b_j^0 e^{-i\omega_j t} e^{\gamma_j t}$, and when replaced in the previous equation, we obtain

$$\begin{aligned} &\left[(\omega_j + i\gamma_j)b_j^0 + i\dot{b_j^0}\right] \\ &\quad = [C_1 + C_3(b_2)]b_j^0 + [C_2 + C_4(b_2)]b_j^{0*} e^{2i\omega_j t} \\ &\quad \approx [C_1 + C_3(b_2)]b_j^0 + C_4(b_2) b_j^{0*} e^{2i\omega_j t}, \end{aligned} \tag{65}$$

where we have considered only resonant terms, i.e., we eliminated a term proportional to C_2. Mode 2 is such that $\tilde{a}_{mj} \neq 0$ for m odd. If we study the stability of mode j such that $\tilde{a}_{mj} \neq 0$ for the case m even, we will have that $C_3(b_2)$ and $C_4(b_2)$ only will have quadratic terms in b_2. The previous statements are valid for $j = 1$, the particular case that we will study.

We consider $C_3(b_2)$ constant and $C_4(b_2)$ proportional to $e^{-2i\omega_2 t}$. In this way, we write $b_j^0 = u_j^0 e^{i(\omega_j - \omega_2)t} \Rightarrow \delta b_j = u_j^0 e^{-i\omega_2 t} e^{\gamma_j t}$, where γ_j should be

$$\gamma_j = \sqrt{|C_4|^2 - [\omega_i - \mathrm{Re}(C_1 + C_3)]^2} + \mathrm{Im}(C_1 + C_3). \tag{66}$$

Figure 14 shows a comparison between the instability current found theoretically from the previous expression and that found numerically, for mode $j = 1$. The analysis is done for a given applied magnetic field and the applied current is varied: the instability current is identified when $\gamma_j = 0$, i.e., when mode j becomes unstable starting an exponential growth. The agreement between theoretical and numerical

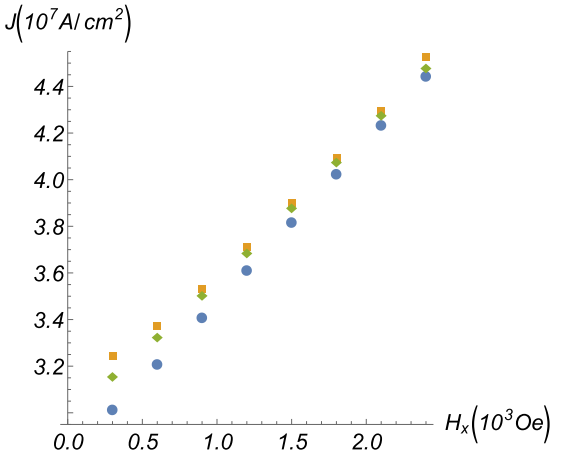

FIG. 14. The circular blue points represent the critical current densities when the mode b_2 starts to auto-oscillate, as a function of applied magnetic field. The square orange and diamond green points represent the instability current densities of the previous auto-oscillatory mode obtained numerically and theoretically, respectively.

results is good, since mode b_2 only attains small amplitudes of oscillation before mode 1 starts to grow.

VI. CONCLUSIONS AND REMARKS

A model for the dynamics of the magnetization of a very thin disk magnetized in plane was developed that under a simplified version (demagnetizing field approximated by its very thin film limit) captures the dynamics of a uniform mode and reproduces the linear nonuniform modes of the system. The idea was to model the dynamics of a free ferromagnetic layer of a nanopillar structure, using a simplified version of the dipolar field that neglects terms proportional to the film thickness. Within this simple version of the model one can also study exactly the dynamics of the uniform mode, or macrospin, when its precession out of equilibrium occurs at large angles, i.e., including all nonlinear terms. Considering a spin transfer torque term and dissipation, at a given critical current density the system develops a periodic macrospin solution, which is an auto-oscillatory limit cycle solution. We obtained an approximate analytic form for this uniform nonlinear periodic solution by neglecting nonresonant terms.

One goal of this work was to determine the linear stability of this mentioned periodic macrospin solution. Using some approximations, we determined analytically the thresholds in current (at a fixed applied magnetic field) at which nonuniform modes of the system become unstable, i.e., points at which the macrospin approximation has to be extended in order to describe the dynamics of the system. The nonuniform modes with lower frequencies are those which become unstable first.

All the previous summarized description of the macrospin dynamics and its stability is valid for applied magnetic fields in plane that do not exceed πM_s in magnitude. For higher applied fields, the picture is a bit more complex: for current densities somewhat below the critical density there is a stable periodic macrospin solution that coexists with the stable static equilibrium uniform solution. There is a gap in energy that separates these two solutions that can easily overcome a thermal excitation energy. We found this coexistence via our analytic results, but an exact numerical simulation of the uniform mode dynamics also shows convergence to this limit cycle solution if one does a significant perturbation of the static equilibrium. The analysis of stability of this higher branch with respect to the growth of nonuniform modes is analogous to the case of lower fields, and one also finds that the lower threshold for instability occurs for the first nonuniform modes. Also, from a practical point of view once the applied field exceeds πM_s the macrospin becomes unstable at a current that is slightly over the thresholds currents for existence of the periodic macrospin solutions.

One aspect of interest of this simplified model was to determine the dependence of the stability of the periodic macrospin solution on the radius of the disk: we found that lower radii correspond to higher stability, something understood in relation to the role of the exchange interaction.

In order to better capture the magnetization dynamics of a real nanometric disk we studied an improved version of the model: we used the full expression of the demagnetizing field. When this is done, the equilibrium magnetization configuration is no longer uniform, and the dynamic linear modes are also modified developing in general features close to the edges of the disk. We did a study of a 50-nm radius disk with this improved model. In particular, there are two modes with similar frequencies at the lower end, the lowest is a quasiuniform mode and the other a mode of edge character. The latter edge mode has the lowest critical current for entering into an auto-oscillatory regime: we studied when this isolated auto-oscillation becomes unstable due to the exponential growth of the quasiuniform mode. In conclusion, this improved model showed us that one can study the full effect of the demagnetizing field within the framework of this model, allowing to determine the different nonlinear terms that contribute to the demagnetizing energy. The improved model reproduces well the linear dynamic magnetization modes, with the added characteristic of understanding their shape and symmetry properties. The inclusion of the full demagnetizing field effectively shows the effect of the finite size of the disk introducing edge effects that clearly influence the magnetization dynamics of small radii disks.

Thus this models allow to understand the isolated auto-oscillations with lowest critical currents of the magnetization of thin film disks magnetized in plane, as well as the currents under which these auto-oscillations become unstable to the growth of other non-uniformly magnetized modes. Thus the models provide a basic understanding of auto-oscillations at low currents.

This work may stimulate further work in the topic of understanding higher nonlinear effects in the dynamics of nanoferromagnetic samples, as it was studied in the past in a ferromagnetic bulk or thin films. Our treatment of the magnetization dynamics based on the dynamics of the amplitudes of the magnetic modes allows to better understand the magnetization dynamics as compared to a micromagnetic approach, specially in order to appreciate the very important role of resonant phenomena.

As far as extending this approach to other geometries, this approach can be used in ferromagnetic wires of rectangular cross sections, or nanosamples of rectangular geometry. It is also plausible to extend it to thin dots with elliptical base. Furthermore, this approach can be generalized to samples of other shapes with nonuniform magnetization configurations, where it may be used if one has calculated numerically the modes (at this moment it is practical for equilibrium magnetization configurations close to uniform ones).

ACKNOWLEDGMENTS

The authors thank A. Núñez for the critical reading of the manuscript. R.E.A. thanks Project Fondecyt 1130192 and Financiamiento Basal para Centros Científicos y Tecnológicos de Excelencia, Project CEDENNA FB0807 (Chile). D.M-A. thanks A.O. León for fruitful discussions and acknowledges financial support from CONICYT Beca Doctorado Nacional 2012, Contract No. 21120160.

APPENDIX A: DEFINITIONS FOR EQUATIONS

1. Definitions for Eq. (35)

The following expressions are associated with the interaction between the large amplitude uniform mode of oscillation and the modes mj:

$$A_{mj} = \left(h_x + 1/2 + h_{\rm ex}^{mj}\right), \tag{A1a}$$

$$B_{mj} = 1/2, \tag{A1b}$$

$$C_{mj} = h_{\rm ex}^{mj}\frac{|a_{00}|^4}{4(2-|a_{00}|^2)} - \left(\frac{3}{8}a_{00}^2 + |a_{00}|^2 + \frac{3}{8}{a_{00}^*}^2\right), \tag{A1c}$$

$$D_{mj} = h_{\rm ex}^{mj}\frac{|a_{00}|^2 a_{00}^2}{4(2-|a_{00}|^2)} + \frac{1}{2}\left(h_{\rm ex}^{mj}-1\right)a_{00}^2 - \frac{3}{4}|a_{00}|^2, \tag{A1d}$$

$$E_{mj} = \frac{3\alpha}{8}\left[3a_{00}^2 + \left(4+\frac{8}{3}h_x\right)|a_{00}|^2 + {a_{00}^*}^2 - \frac{2}{3}\left(2a_{00}^2 + 3|a_{00}|^2 + {a_{00}^*}^2\right)|a_{00}|^2\right] - \beta J|a_{00}|^2, \tag{A1e}$$

$$F_{mj} = \frac{3\alpha}{4}\left[\left(1+\frac{2}{3}h_x\right)a_{00}^2 + |a_{00}|^2 - \frac{1}{6}\left(a_{00}^2 + 4|a_{00}|^2 + 3{a_{00}^*}^2\right)a_{00}^2\right] - \frac{\beta J}{2}a_{00}^2. \tag{A1f}$$

For the theoretical analysis, we approximate the terms associated with the exchange interaction as

$$C_{mj} \approx \frac{h_{\rm ex}^{mj}}{8}|a_{00}|^4 - \left(\frac{3}{8}a_{00}^2 + |a_{00}|^2 + \frac{3}{8}{a_{00}^*}^2\right), \tag{A2a}$$

$$D_{mj} \approx \frac{h_{\rm ex}^{mj}}{8}|a_{00}|^2 a_{00}^2 + \frac{1}{2}\left(h_{\rm ex}^{mj}-1\right)a_{00}^2 - \frac{3}{4}|a_{00}|^2. \tag{A2b}$$

2. Definitions for Eq. (36)

In doing the change of variables from the a_{mj} to the b_{mj}, it is convenient to define the following quantities:

$$G_{mj} = \frac{A_{mj}(C_{mj}+C_{mj}^*)}{2\omega_{mj}} - \frac{B_{mj}(D_{mj}+D_{mj}^*)}{2\omega_{mj}} + \frac{C_{mj}-C_{mj}^*}{2}, \tag{A3a}$$

$$H_{mj} = \frac{A_{mj}(E_{mj}-E_{mj}^*)}{2\omega_{mj}} - \frac{B_{mj}(F_{mj}-F_{mj}^*)}{2\omega_{mj}} + \frac{E_{mj}+E_{mj}^*}{2}, \tag{A3b}$$

$$I_{mj} = \frac{A_{mj}(D_{mj}+D_{mj}^*)}{2\omega_{mj}} - \frac{B_{mj}(C_{mj}+C_{mj}^*)}{2\omega_{mj}} + \frac{D_{mj}-D_{mj}^*}{2}, \tag{A3c}$$

$$J_{mj} = \frac{A_{mj}(F_{mj}-F_{mj}^*)}{2\omega_{mj}} - \frac{B_{mj}(E_{mj}-E_{mj}^*)}{2\omega_{mj}} + \frac{F_{mj}+F_{mj}^*}{2}. \tag{A3d}$$

3. Definitions for Eq. (39)

In searching for a solution to the b_{mj}^0 that varies slowly in time, we may neglect some contributions to the terms G_{mj}, H_{mj}, I_{mj} and J_{mj}. We define G'_{mj}, H'_{mj}, I'_{mj}, and J'_{mj} as a result of this process:

$$G'_{mj} = \frac{1}{2\omega_{mj}}[A_{mj}(C'_{mj}+{C'}^*_{mj}) - B_{mj}(D'_{mj}+{D'}^*_{mj})], \tag{A4a}$$

$$H'_{mj} = \frac{E'_{mj} + E'^{*}_{mj}}{2}. \tag{A4b}$$

The terms G'_{mj} and H'_{mj} correspond to the terms that do not depend on time in G_{mj} and H_{mj}, with

$$C'_{mj} + C'^{*}_{mj} \approx \left(\frac{3B_{00} - 4A_{00}}{2\omega_{00}}\right) + h_{\text{ex}}^{mj}\left(\frac{2A_{00}^2 + B_{00}^2}{8\omega_{00}^2}\right)|b_{00}|^2, \tag{A5a}$$

$$D'_{mj} + D'^{*}_{mj} \approx (1 - h_{\text{ex}}^{mj})\left(\frac{B_{00}}{\omega_{00}}\right) - \frac{3A_{00}}{2\omega_{00}} - 3h_{\text{ex}}^{mj}\frac{A_{00}B_{00}}{8\omega_{00}^2}|b_{00}|^2, \tag{A5b}$$

$$E'_{mj} + E'^{*}_{mj} = \alpha\left[2\frac{(3B_{00} + A_{00})(A_{00} - B_{00})}{\omega_{00}} - 3\frac{(2A_{00} - B_{00})(A_{00} - B_{00})}{4\omega_{00}^2}|b_{00}|^2\right] - 2\beta J\frac{A_{00}}{\omega_{00}}, \tag{A5c}$$

$$I'_{mj} = \frac{A_{mj}(d_{mj} + d^{*}_{mj})}{2\omega_{mj}} - \frac{B_{mj}(c_{mj} + c^{*}_{mj})}{2\omega_{mj}} + \frac{1}{2}(d_{mj} - d^{*}_{mj}), \tag{A6a}$$

$$J'_{mj} = \frac{A_{mj}(f_{mj} - f^{*}_{mj})}{2\omega_{mj}} - \frac{B_{mj}(e_{mj} - e^{*}_{mj})}{2\omega_{mj}} + \frac{1}{2}(f_{mj} + f^{*}_{mj}). \tag{A6b}$$

The terms I'_{mj} and J'_{mj} correspond to the terms proportional to $e^{-2i\omega t'}$ in I_{mj} and J_{mj} with

$$c_{mj} + c^{*}_{mj} \approx -h_{\text{ex}}^{mj}\frac{A_{00}B_{00}}{4\omega_{00}^2}|b_{00}|^2 - \left(\frac{3A_{00} - 4B_{00}}{4\omega_{00}}\right), \tag{A7a}$$

$$d_{mj} + d^{*}_{mj} \approx h_{\text{ex}}^{mj}\frac{A_{00}^2 + B_{00}^2}{8\omega_{00}^2}|b_{00}|^2 + \frac{1}{2}\left(h_{\text{ex}}^{mj} - 1\right)\frac{A_{00}}{\omega_{00}} + \frac{3B_{00}}{4\omega_{00}}, \tag{A7b}$$

$$d_{mj} - d^{*}_{mj} \approx h_{\text{ex}}^{mj}\frac{A_{00}}{8\omega_{00}}|b_{00}|^2 + \frac{1}{2}\left(h_{\text{ex}}^{mj} - 1\right), \tag{A7c}$$

$$e_{mj} - e^{*}_{mj} = \alpha\left(\frac{3}{4} - \frac{A_{00}}{4\omega_{00}}|b_{00}|^2\right), \tag{A7d}$$

$$f_{mj} + f^{*}_{mj} = \alpha\left[\frac{(A_{00} + 3B_{00})(A - B_{00})}{2\omega_{00}} - \frac{(A_{00} - B_{00})^2}{2\omega_{00}^2}|b_{00}|^2\right] - \frac{\beta J}{2}\frac{A_{00}}{\omega_{00}}, \tag{A7e}$$

$$f_{mj} - f^{*}_{mj} = \alpha\left(\frac{A_{00} + 2B_{00}}{2} + \frac{B_{00} - 2A_{00}}{4\omega_{00}}|b_{00}|^2\right) - \frac{\beta J}{2}. \tag{A7f}$$

APPENDIX B: DEMAGNETIZING FIELD AND DEMAGNETIZING ENERGY

To determine the demagnetizing field of our thin disk (the magnetization is assumed uniform over the thickness of the disk) we first calculate the magnetostatic potential ($\vec{H}_D = -\vec{\nabla}\phi$), which has contributions from surface and volume effective magnetic charges:

$$\Phi(\vec{x}) = \int dS' \frac{\hat{n}\cdot\vec{M}(\vec{x'})}{|\vec{x} - \vec{x}'|} - \int dV' \frac{\vec{\nabla}\cdot\vec{M}(\vec{x'})}{|\vec{x} - \vec{x'}|}. \tag{B1}$$

$\sigma_M = (\hat{n}\cdot\vec{M})$ represents the surface magnetic charge density, with contributions from the top and bottom surfaces of the disk and from its mantle; and $\rho_M = -(\nabla\cdot\vec{M})$ the volumetric magnetic charge density, with contributions from the interior of the disk.

In order to calculate these potentials, we use the following representation of the Green's function in terms of cylindrical coordinates:

$$\frac{1}{|\vec{x} - \vec{x}'|} = \sum_{m=-\infty}^{\infty} e^{im(\phi - \phi')}\int_0^{\infty} dk\, J_m(k\rho)J_m(k\rho')e^{-k|z - z'|}. \tag{B2}$$

The demagnetizing field averaged over the thickness of the disk can be separated into two parts. (a) Its component in the perpendicular direction to the plane z, with contribution only from surface charges in the top and bottom surfaces:

$$H^{z}_{\text{dem}} = -4\pi M_z(\rho,\phi) + \frac{2M_s}{h}\int_0^{\infty} dk f(kh)\sum_{m=-\infty}^{\infty}\left[\int dS' J_m(k\rho')m_z(\rho',\phi')e^{-im\phi'}\right]J_m(k\rho)e^{im\phi}, \tag{B3}$$

with $f(u) \equiv \exp(-u) - 1 + u$.

(b) Its in plane components, with contributions from mantle surface charges as well as volume charges:

$$\vec{H}_{\rm dem}^{\perp} = -\frac{2M_s}{h}\int_0^{\infty} dk\,\frac{f(kh)}{k^2}\sum_{m=-\infty}^{\infty}\left[\int dS'\vec{\nabla}(J_m(k\rho')e^{-im\phi'})\cdot\vec{m}(\rho',\phi')\right]\vec{\nabla}(J_m(k\rho)e^{im\phi}). \tag{B4}$$

Furthermore, the demagnetizing energy is calculated in the following form:

$$\mathcal{U} = -\frac{1}{8\pi M_s^2}\int\left[H_{\rm dem}^{z}\hat{z} + \vec{H}_{\rm dem}^{\perp}\right]\cdot\vec{M}dV. \tag{B5}$$

We write the magnetization components in the following way ($M_{\pm} \equiv M_x \pm iM_y$):

$$\begin{aligned} M_z &= M_s\sum_{lj}\sigma_{lj}N_{lj}J_l(\kappa_{lj}\rho)e^{il\phi},\\ M_{\pm} &= M_s\sum_{lj}\sigma_{lj}^{\pm}N_{lj}J_l(\kappa_{lj}\rho)e^{il\phi}. \end{aligned} \tag{B6}$$

Using equations (B3)–(B6), one obtains the demagnetizing energy as follows, $\mathcal{U} = \mathcal{U}^z + \mathcal{U}^{\perp}$, with

$$\mathcal{U}^z = \frac{1}{2}\sum_{l_1 j_1 j_2}(-1)^{l_1}\sigma_{l_1 j_1}^{z}\sigma_{-l_1 j_2}^{z}\left(\delta_{j_2}^{j_1} - 2VI_{(l_1,j_1,j_2,h/R)}^{1}\right), \tag{B7}$$

$$\mathcal{U}^{\perp} = -\frac{V}{4}\sum_{l_1 j_1 j_2}(-1)^{l_1}\left(\sigma_{l_1 j_1}^{-}\sigma_{(-l_1-2)j_2}^{-}I_{(l_1,j_1,j_2,h/R)}^{2} + \sigma_{l_1 j_1}^{+}\sigma_{(-l_1+2)j_2}^{+}I_{(l_1,j_1,j_2,h/R)}^{3} - 2\sigma_{l_1 j_1}^{+}\sigma_{(-l_1)j_2}^{-}I_{(l_1,j_1,j_2,h/R)}^{1}\right), \tag{B8}$$

where the σ_{lj}^{z}, σ_{lj}^{+}, and σ_{lj}^{-} are functions of the variables a_{mj} [see Eqs. (3) and (7)], with details of these expressions in Sec. B 1; and the $I_{(l_1,j_1,j_2,h/R)}^{1}$, $I_{(l_1,j_1,j_2,h/R)}^{2}$, $I_{(l_1,j_1,j_2,h/R)}^{3}$ represent integrals that are calculated numerically, with details in Sec. B 2. In the limit $h/R \to 0$, the previous integrals tend to zero, and then the demagnetizing energy takes the value valid for an infinite very thin film:

$$\mathcal{U} \to \frac{1}{2}\sum_{l_1 j_1}(-1)^{l_1}\sigma_{l_1 j_1}^{z}\sigma_{-l_1 j_1}^{z} = \frac{1}{2}\int m_z(\rho,\phi)^2 dV. \tag{B9}$$

1. Relation between the $\sigma'_{lj}s$ and the $a'_{mj}s$

The $\sigma'_{lj}s$ [defined through Eq. (B6)] are functions of the $a'_{mj}s$ [defined through Eqs. (3) and (7)]. These may be expanded in power series of the $a'_{mj}s$ as follows (superindices indicate the order of approximation):

$$\sigma_{lj}^{z\,(0)} = 0 = \sigma_{lj}^{z\,(2)} = \sigma_{lj}^{z\,(4)}, \tag{B10a}$$

$$\sigma_{lj}^{z\,(1)} = (a_{lj} + (-1)^l a_{-lj}^{*})/\sqrt{2}, \tag{B10b}$$

$$\sigma_{lj}^{z\,(3)} = -\frac{V}{2\sqrt{2}}\sum_{m_1 j_1 m_2 j_2 m_3 j_3}(a_{m_1 j_1} + (-1)^{m_1}a_{-m_1 j_1}^{*})a_{m_2 j_2}a_{m_3 j_3}^{*}i_{ljm_1 j_1 m_2 j_2 m_3 j_3}^{4}\delta_{m_3}^{m_1+m_2-l}, \tag{B10c}$$

$$\sigma_{00}^{z\,(0)} = \sigma_{00}^{+(0)} = \sigma_{00}^{-(0)} = \sqrt{V}, \tag{B10d}$$

$$\sigma_{lj}^{+(1)} = -\sigma_{lj}^{-(1)} = (a_{lj} - (-1)^l a_{-lj}^{*})/\sqrt{2}, \tag{B10e}$$

$$\sigma_{lj}^{+(2)} = \sigma_{lj}^{-(2)} = -2\sum_{m_1 j_1 m_2 j_2}a_{m_1 j_1}a_{m_2 j_2}^{*}\delta_{m_2}^{m_1-l}i_{d(ljm_1 j_1 m_2 j_2)}^{3}, \tag{B10f}$$

$$\sigma_{lj}^{+(3)} = -\sigma_{lj}^{-(3)} = \sigma_{lj}^{z\,(3)}, \tag{B10g}$$

$$\sigma_{lj}^{+(4)} = \sigma_{lj}^{-(4)} = 0 \tag{B10h}$$

with $i_{d(ljm_1 j_1 m_2 j_2)}^{3}$ and $i_{d(ljm_1 j_1 m_2 j_2)}^{4}$ integrals defined in Sec. B 2.

2. Integrals calculated numerically

$$I^1_{(l_1,j_1,j_2,h/R)} = N_{l_1 j_1} N_{l_1 j_2} J_{l_1}\left(\chi^{l_1}_{j_1}\right) J_{l_1}\left(\chi^{l_1}_{j_2}\right) \int_0^\infty dk \frac{f(kh/R) k^2 J'_{l_1}(k)^2}{(h/R)\left(k^2 - \left(\chi^{l_1}_{j_1}\right)^2\right)\left(k^2 - \left(\chi^{l_1}_{j_2}\right)^2\right)}, \tag{B11a}$$

$$I^2_{(l_1,j_1,j_2,h/R)} = N_{l_1 j_1} N_{(l_1+2) j_2} J_{l_1}\left(\chi^{l_1}_{j_1}\right) J_{l_1+2}\left(\chi^{l_1+2}_{j_2}\right) \int_0^\infty dk \frac{f(kh/R) k^2 J'_{l_1}(k) J'_{l_1+2}(k)}{(h/R)\left(k^2 - \left(\chi^{l_1}_{j_1}\right)^2\right)\left(k^2 - \left(\chi^{l_1+2}_{j_2}\right)^2\right)}, \tag{B11b}$$

$$I^3_{(l_1,j_1,j_2,h/R)} = N_{l_1 j_1} N_{(l_1-2) j_2} J_{l_1}\left(\chi^{l_1}_{j_1}\right) J_{l_1-2}\left(\chi^{l_1-2}_{j_2}\right) \int_0^\infty dk \frac{f(kh/R) k^2 J'_{l_1}(k) J'_{l_1-2}(k)}{(h/R)\left(k^2 - \left(\chi^{l_1}_{j_1}\right)^2\right)\left(k^2 - \left(\chi^{l_1-2}_{j_2}\right)^2\right)}, \tag{B11c}$$

$$i^3_{d(ljm_1 j_1 m_2 j_2)} = N_{lj} N_{m_1 j_1} N_{m_2 j_2} \int_0^1 J_l(\chi^l_j x) J_{m_1}\left(\chi^{m_1}_{j_1} x\right) J_{m_2}\left(\chi^{m_2}_{j_2} x\right) x dx, \tag{B12}$$

$$i^4_{d(ljm_1 j_1 m_2 j_2 m_3 j_3)} = N_{lj} N_{m_1 j_1} N_{m_2 j_2} N_{m_3 j_3} \int_0^1 J_l\left(\chi^l_j x\right) J_{m_1}\left(\chi^{m_1}_{j_1} x\right) J_{m_2}\left(\chi^{m_2}_{j_2} x\right) J_{m_3}\left(\chi^{m_3}_{j_3} x\right) x dx. \tag{B13}$$

[1] J. C. Slonczewski, Current-driven excitation of magnetic multilayers, J. Magn. Magn. Mater. **159**, L1 (1996).

[2] L. Berger, Emission of spin waves by a magnetic multilayer traversed by a current, Phys. Rev. B **54**, 9353 (1996).

[3] F. J. Albert, J. A. Katine, R. A. Buhrman, and D. C. Ralph, Spin-polarized current switching of a Co thin film nanomagnet, Appl. Phys. Lett. **77**, 3809 (2000).

[4] E. B. Myers, D. C. Ralph, J. A. Katine, R. N. Louie, and R. A. Buhrman, Current-induced switching of domains in magnetic multilayer devices, Science **285**, 867 (1999).

[5] J. A. Katine, F. J. Albert, R. A. Buhrman, E. B. Myers, and D. C. Ralph, Current-Driven Magnetization Reversal and Spin-Wave Excitations in Co /Cu /Co Pillars, Phys. Rev. Lett. **84**, 3149 (2000).

[6] S. I. Kiselev, J. C. Sankey, I. N. Krivorotov, N. C. Emley, R. J. Scheolkopf, R. A. Buhrman, and D. C. Ralph, Microwave oscillations of a nanomagnet driven by a spin-polarized current, Nature (London) **425**, 380 (2003).

[7] W. H. Rippard, M. R. Pufall, S. Kaka, S. E. Russek, and T. J. Silva, Direct-Current Induced Dynamics in Co90Fe10/Ni80Fe20 Point Contacts, Phys. Rev. Lett. **92**, 027201 (2004).

[8] I. N. Krivorotov, N. C. Emley, J. C. Sankey, S. I. Kiselev, D. C. Ralph, and R. A. Buhrman, Time-domain measurements of nanomagnet dynamics driven by spin-transfer torques, Science **307**, 228 (2005).

[9] T. Kawahara, K. Ito, R. Takemura, and H. Ohno, Spin-transfer torque RAM technology: Review and prospect, Microelectron. Reliab. **52**, 613 (2012).

[10] E. Chen, D. Apalkov, Z. Diao, A. Driskill-Smith, D. Druist, D. Lottis, V. Nikitin, X. Tang, S. Watts, S. Wang, S. A. Wolf, A. W. Ghosh, J. W. Lu, S. J. Poon, M. Stan, W. H. Butler, S. Gupta, C. K. A. Mewes, T. Mewes, and P. B. Visscher, Advances and future prospects of spin-transfer torque random access memory, IEEE Trans. Magn. **46**, 1873 (2010).

[11] J. A. Katine and E. E. Fullerton, Device implications of spin-transfer torques, J. Magn. Magn. Mater. **320**, 1217 (2008).

[12] M. R. Pufall, W. H. Rippard, S. Kaka, T. J. Silva, and S. E. Russek, Frequency modulation of spin-transfer oscillators, Appl. Phys. Lett. **86**, 082506 (2005).

[13] J. Z. Sun, Spin-current interaction with a monodomain magnetic body: A model study, Phys. Rev. B **62**, 570 (2000).

[14] Jiang Xiao, A. Zangwill, and M. D. Stiles, Macrospin models of spin transfer dynamics, Phys. Rev. B **72**, 014446 (2005).

[15] U. Ebels, D. Houssameddine, I. Firastrau, D. Gusakova, C. Thirion, B. Dieny, and L. D. Buda-Prejbeanu, Macrospin description of the perpendicular polarizer-planar free-layer spin-torque oscillator, Phys. Rev. B **78**, 024436 (2008).

[16] Z. Li and S. Zhang, Magnetization dynamics with a spin-transfer torque, Phys. Rev. B **68**, 024404 (2003).

[17] M. D. Stiles and J. Miltat, *Spin Transfer Torque and Dynamics, in Spin Dynamics in Confined Magnetic Structures III*, edited by B. Hillebrands and A. Thiaville (Springer-Verlag, Berlin-Heidelberg, 2006), Sec. 4.

[18] S. I. Kiselev, J. C. Sankey, I. N. Krivorotov, N. C. Emley, M. Rinkoski, C. Perez, R. A. Buhrman, and D. C. Ralph, Current-Induced Nanomagnet Dynamics for Magnetic Fields Perpendicular to the Sample Plane, Phys. Rev. Lett. **93**, 036601 (2004).

[19] R. H. Koch, J. A. Katine, and J. Z. Sun, Time-Resolved Reversal of Spin-Transfer Switching in a Nanomagnet, Phys. Rev. Lett. **92**, 088302 (2004).

[20] D. V. Berkov and J. Miltat, Spin-torque driven magnetization dynamics: Micromagnetic modeling, J. Magn. Magn. Mater. **320**, 1238 (2008).

[21] K. J. Lee, A. Deac, O. Redon, J-P. Nozieres, and B. Dieny, Excitations of incoherent spin-waves due to spin-transfer torque, Nat. Mater. **3**, 877 (2004).

[22] D. V. Berkov and N. L. Gorn, Magnetization precession due to a spin-polarized current in a thin nanoelement: Numerical simulation study, Phys. Rev. B **72**, 094401 (2005).

[23] E. Schlomann and J. J. Green, Ferromagnetic Resonance at High Power Levels, Phys. Rev. Lett. **3**, 129 (1959).

[24] V. S. L'vov, *Wave Turbulence Under Parametric Excitation* (Springer-Verlag, Berlin, 1994).

[25] P. Krivosik and C. E. Patton, Hamiltonian formulation of nonlinear spin-wave dynamics: Theory and applications, Phys. Rev. B **82**, 184428 (2010).
[26] S. M. Rezende, F. M. de Aguiar, and A. Azevedo, Spin-Wave Theory for the Dynamics Induced by Direct Currents in Magnetic Multilayers, Phys. Rev. Lett. **94**, 037202 (2005).
[27] A. N. Slavin and P. Kabos, Approximate theory of microwave generation in a current-driven magnetic nanocontact magnetized in an arbitrary direction, IEEE Trans. Magn. **41**, 1264 (2005).
[28] G. Bertotti, R. Bonin, M. d'Aquino, C. Serpico, and I. D. Mayergoyz, Spin-wave instabilities in spin-transfer-driven magnetization dynamics, IEEE Magn. Lett. **1**, 3000104 (2010).
[29] R. Bonin, M. d'Aquino, G. Bertotti, C. Serpico, and I. D. Mayergoyz, Stability of magnetization oscillations driven by spin-polarized currents, J. Appl. Phys. **109**, 07C902 (2011).
[30] M. Pauselli and G. Carlotti, Spin wave eigenmodes excited by spin transfer torque in circular nanopillars: influence of lateral size and Oersted field studied by micromagnetic simulations, J. Phys. D: Appl. Phys. **48**, 415001 (2015).
[31] G. Carlotti, G. Gubbiotti, M. Madami, S. Tacchi, F. Hartmann, M. Emmerling, M. Kamp, and L. Worschech, From micro to nano-magnetic dots: evolution of the eigenmodes spectrum on reducing the lateral size, J. Phys. D: Appl. Phys. **47**, 265001 (2014).
[32] D. L. Mills and J. A. C. Bland, *Nanomagnetism: Ultrathin Films, Multilayers and Nanostructures* (Elsevier, Amsterdam, 2006), Chap. 3.
[33] J. C. Slonczewski, Currents and torques in metallic magnetic multilayers, J. Magn. Magn. Mater. **247**, 324 (2002).
[34] L. D. Landau and E. M. Lifshitz, On the theory of the dispersion of magnetic permeability in ferromagnetic bodies, Phys. Z. Sowjetunion **8**, 153 (1935) [Ukr. J. Phys. **53**, 14 (2008)].
[35] H. J. Suhl, The theory of ferromagnetic resonance at high signal powers, Phys. Chem. Solids **1**, 209 (1957).
[36] T. Holstein and H. Primakoff, Field dependence of the intrinsic domain magnetization of a ferromagnet, Phys. Rev. **58**, 1098 (1940).
[37] W. S. Ament and G. T. Rado, Electromagnetic effects of spin wave resonance in ferromagnetic metals, Phys. Rev. **97**, 1558 (1955).
[38] A. Slavin and V. Tiberkevich, Excitation of spin waves by spin-polarized current in magnetic nano-structures, IEEE Trans. Magn. **44**, 1916 (2008).
[39] A. N. Slavin and V. S. Tiberkevich, Current-induced bistability and dynamic range of microwave generation in magnetic nanostructures, Phys. Rev. B **72**, 094428 (2005).
[40] Q. Mistral, J. V. Kim, T. Devolder, P. Crozat, C. Chappert, J. A. Katine, M. J. Carey, and K. Ito, Current-driven microwave oscillations in current perpendicular-to-plane spin-valve nanopillars, Appl. Phys. Lett. **88**, 192507 (2006).
[41] J. V. Kim, V. Tiberkevich, and A. N. Slavin, Generation Linewidth of an Auto-Oscillator with a Nonlinear Frequency Shift: Spin-Torque Nano-Oscillator, Phys. Rev. Lett. **100**, 017207 (2008).
[42] A. Slavin and V. Tiberkevich, Nonlinear auto-oscillator theory of microwave generation by spin-polarized current, IEEE Trans. Magn. **45**, 1875 (2009).
[43] A. O. León and M. G. Clerc, Spin-transfer-driven nano-oscillators are equivalent to parametric resonators, Phys. Rev. B **91**, 014411 (2015).
[44] M. G. Clerc, S. Coulibaly, D. Laroze, A. O. León, and A. S. Núñez, Alternating spin-polarized current induces parametric resonance in spin valves, Phys. Rev. B **91**, 224426 (2015).
[45] I. D. Mayergoyz, G. Bertotti, and C. Serpico, *Nonlinear Magnetization Dynamics in Nanosystems* (Elsevier, Oxford, 2009).
[46] E. T. Jaynes and F. W. Cummings, Proc. IEEE **51**, 89 (1963).
[47] E. K. Irish, J. Gea-Banacloche, I. Martin, and K. C. Schwab, Dynamics of a two-level system strongly coupled to a high-frequency quantum oscillator, Phys. Rev. B **72**, 195410 (2005).
[48] Steven Strogatz, *Nonlinear Dynamics and Chaos: With Applications to Physics, Biology, Chemistry and Engineering* (Perseus Books Group, Massachusetts, 2000).
[49] Z. Zeng, K. H. Cheung, H. W. Jiang, I. N. Krivorotov, J. A. Katine, V. Tiberkevich, and A. Slavin, Evolution of spin-wave modes in magnetic tunnel junction nanopillars, Phys. Rev. B **82**, 100410 (2010).
[50] E. Iacocca, O. Heinonen, P. K. Muduli, and J. Åkerman, Generation linewidth of mode-hopping spin torque oscillators, Phys. Rev. B **89**, 054402 (2014).
[51] P. K. Muduli, O. G. Heinonen, and J. Akerman, Decoherence and Mode Hopping in a Magnetic Tunnel Junction Based Spin Torque Oscillator, Phys. Rev. Lett. **108**, 207203 (2012).
[52] O. G. Heinonen, P. K. Muduli, E. Iacocca, and J. Akerman, Decoherence, mode hopping, and mode coupling in spin torque oscillators, IEEE Trans. Magn. **49**, 4398 (2013).
[53] R. I. Joseph and E. Schlomann, Demagnetizing Field in Nonellipsoidal Bodies, J. Appl. Phys. **36**, 1579 (1965).
[54] K. Yu. Guslienko and A. N. Slavin, Spin-waves in cylindrical magnetic dot arrays with in-plane magnetization, J. Appl. Phys. **87**, 6337 (2000).
[55] R. Zivieri and R. L. Stamps, Theory of spin wave modes in tangentially magnetized thin cylindrical dots: A variational approach, Phys. Rev. B **73**, 144422 (2006).
[56] R. Zivieri, G. Santoro, and A. Franchini, Localized spin modes in ferromagnetic cylindrical dots with in-plane magnetization, J. Phys.: Condens. Matter **19**, 305012 (2007).
[57] G. Strang, *Introduction to Applied Mathematics* (Wellesley-Cambridge, Wellesley, 1986), Chap. 5, pp. 373-380.
[58] D. T. DiPerna and T. K. Stanton, Sound scattering by cylinders of noncircular cross section: A conformal mapping approach, J. Acoust. Soc. Am. **96**, 3064 (1994).
[59] W. Scholza, K. Yu. Guslienkob, V. Novosadc, D. Suessa, T. Schrefla, R. W. Chantrellb, and J. Fidler, Transition from single-domain to vortex state in soft magnetic cylindrical nanodots, J. Magn. Magn. Mater. **266**, 155 (2008).
[60] S.-H. Chung, R. D. McMichael, D. T. Pierce, and J. Unguris, Phase diagram of magnetic nanodisks measured by scanning electron microscopy with polarization analysis, Phys. Rev. B **81**, 024410 (2010).
[61] B. A. Ivanov and C. E. Zaspel, Magnonmodes for thin circular vortex state magnetic dots, Appl. Phys. Lett. **81**, 1261 (2002).
[62] B. A. Ivanov, H. J. Schnitzer, F. G. Mertens, and G. M. Wysin, Magnon modes and magnon-vortex scattering in

two-dimensional easy-plane ferromagnets, Phys. Rev. B **58**, 8464 (1998).

[63] C. E. Zaspel, B. A. Ivanov, J. P. Park, and P. A. Crowell, Excitations in vortex-state Permalloy dots, Phys. Rev. B **72**, 024427 (2005).

[64] M. Buess, T. P. J. Knowles, R. Höllinger, T. Haug, U. Krey, D. Weiss, D. Pescia, M. R. Scheinfein, and C. H. Back, Excitations with negative dispersion in a spin vortex, Phys. Rev. B **71**, 104415 (2005).

[65] L. Giovannini, F. Montoncello, F. Nizzoli, G. Gubbiotti, G. Carlotti, T. Okuno, T. Shinjo, and M. Grimsditch, Spin excitations of nanometric cylindrical dots in vortex and saturated magnetic states, Phys. Rev. B **70**, 172404 (2004).

[66] G. Consolo, L. Giovannini, and R. Zivieri, Excitation of magnetic normal modes by spin-torque: a Lagrangian approach, J. Appl. Phys. **111**, 07C916 (2012).